

# UCLA

## UCLA Previously Published Works

### Title

An assessment of potential climate impact during 1948–2010 using historical land use land cover change maps

### Permalink

<https://escholarship.org/uc/item/4fq4042q>

### Journal

International Journal of Climatology, 41(1)

### ISSN

0899-8418

### Authors

Chilukoti, Nagaraju  
Xue, Yongkang

### Publication Date

2021

### DOI

10.1002/joc.6621

Peer reviewed

**RESEARCH ARTICLE**

# An assessment of potential climate impact during 1948–2010 using historical land use land cover change maps

Nagaraju Chilukoti<sup>1,2</sup>  | Yongkang Xue<sup>1</sup>

<sup>1</sup>Department of Geography, University of California Los Angeles, Los Angeles, California

<sup>2</sup>National Institute of Technology Rourkela, Rourkela, Odisha, India

**Correspondence**

Nagaraju Chilukoti, Department of Geography, University of California Los Angeles, Los Angeles, CA.  
Email: chilukotinagaraju@gmail.com

**Funding information**

Division of Atmospheric and Geospace Sciences, Grant/Award Number: AGS-1419526

**Abstract**

Earlier studies of land use land cover change (LULCC) normally used only a specified LULCC map with no interannual variations. In this study, using an Atmospheric General Circulation Model (AGCM) coupled with a land surface model, biophysical impacts of LULCC on global and regional climate are investigated by using a LULCC map which covers 63 years from 1948 to 2010 with interannual variation. A methodology has been developed to convert a recently developed LULCC fraction map with  $1^\circ \times 1^\circ$  resolution to the AGCM grid points in which only one dominant type is allowed. Comprehensive evaluations are conducted to ensure consistency of the trend of the original LULCC fraction change and the trend of the fraction of grid point changes over different regions. The model was integrated with a potential vegetation map (CTL) and the map with LULCC, in which a set of surface parameters such as leaf area index, albedo and other soil and vegetation parameters were accordingly changed with interannual variation. The results indicate that the interannual LULCC map simulation is able to reproduce better interannual variability of surface temperature and rainfall when compared to the control simulation. LULCC causes negative effect on global precipitation, with the strongest significant signals over degraded regions such as East Asia, West Africa and South America, and some of these changes are consistent with observed regional anomalies for certain time periods. LULCC causes reduction in net radiation and evapotranspiration which leads to changes in monsoon circulation and variation in magnitude and pattern of moisture flux convergence and subsequent reduction in precipitation. Meanwhile, LULCC enhances surface warming during the summer in the LULCC regions due to greatly reduced evapotranspiration. In contradiction to the surface, upper troposphere temperatures are cool because of less latent heat released into the upper troposphere, which leads to weaker circulation in LULCC regions.

**KEYWORDS**

land use land cover change, land–atmosphere interactions, monsoon, precipitation reduction, surface energy balance

## 1 | INTRODUCTION

Human activities over the last three centuries had a significant impact on Earth's environment. While the effect of greenhouse gases has been comprehensively studied, the effects of human-induced land use land cover changes (LULCCs) are still elusive (Pitman *et al.*, 2009; Boone *et al.*, 2016; Sy *et al.*, 2017). Increased human population and per capita consumption of resources in the last three centuries has led to a widespread modification of Earth's biosphere and atmospheric composition (Vitousek *et al.*, 1997; Wackernagel *et al.*, 1999). One of the primary exercises causing LULCC is the conversion of natural ecosystems to agriculture, rangeland, industrial land and urban areas. There has been increasing recognition of these changes and the consequent environmental damage, as well as of the rapid depletion of natural resources (Marsh, 1864; Thomas, 1956; Pielke *et al.*, 2011; Duveiller *et al.*, 2018). LULCC leads to an adverse effect on the environment such as water resource deterioration, soil degradation and poor air quality (Borrego *et al.*, 2006; Cho and Choi, 2014; Cárdenas Rodríguez *et al.*, 2016; Sun *et al.*, 2016). LULCC plays a vital role in surface energy, momentum, heat, water and biogeochemical balances. It affects regional weather and climate through impacts on the surface albedo, surface roughness and other vegetation and soil properties, as well as partitioning of available energy between latent and sensible heat and partitioning of rainfall between evaporation and runoff (Xue, 1997; Pitman, 2003; Xue, De Sales, Vasic, *et al.*, 2010; Pielke *et al.*, 2011). The fifth assessment report of the Intergovernmental Panel on Climate Change (IPCC; Myhre *et al.*, 2013) highlighted that global land-use change has led to a change in radiative forcing due to increased land surface albedo, which in turn causes variations in the land surface temperature (LST). As such, accurate representation of LULCC is necessary to improve understanding of its effect.

Previous studies have shown that LULCC has played a significant role in decreasing moderate rainfall events in monsoon regions (Schilling *et al.*, 2009; Halder *et al.*, 2016; Rodgers *et al.*, 2018). Halder *et al.* (2016) noted that LULCC contributed to the increase in extreme rainfall and temperature events over India. Similarly, land degradation in Mongolian and inner Mongolian grasslands and the Sahel have an effect on the northeast Asian monsoon and the West African monsoon, respectively (Xue and Shukla, 1993; Xue, 1996, 1997; Xue and Shukla, 1996). Using a hypothetical land cover change map over the Sahel region, Xue (1997) shows that in the degraded areas surface temperature increased and rainfall decreased, whereas the rainfall increased to the south of the degraded areas. Changes in latent heat and

moisture convergence play a dominant role and radiative cooling is a secondary effect over degraded areas (Xue, 1997; Clark *et al.*, 2001). A Northern African study has shown that surface warming and weakening of the hydrological cycle over tropical Africa is mainly due to land degradation when compared to the greenhouse gas effect (Paeth *et al.*, 2009). In a recent study using a hypothetical LULCC map, Bamba *et al.* (2018) explored the effect of reforestation location on West African climate. It revealed that replacing standard vegetation with a hypothetical reforestation belt around 15°N latitude over the West African monsoon region increased rainfall and induced cooler temperatures over that region compared to the incorporation of a reforestation belt around 10°N latitude, highlighting the importance of land-atmospheric interactions and their complex feedbacks. Also, there are some controversies regarding the LULCC effect on surface temperature. The impact of LULCC on LST may vary with location. In tropical and temperate regions, LULCC can lead to a surface warming via reduced evapotranspiration, whereas in high-latitude regions, such as Europe and North America, LULCC can result in surface cooling primarily because of increased land surface albedo (Shukla *et al.*, 1990; Niyogi *et al.*, 2002; Davin and de Noblet-Ducoudre, 2010; De Noblet-Ducoudre *et al.*, 2012; Sy *et al.*, 2017; Winckler *et al.*, 2019). Over South America, a conversion of grass to agriculture leads to cooler and wetter near-surface atmospheric conditions, and conversion of wooded grasslands or forest to agriculture leads to warmer temperatures (Beltrán-Przekurat *et al.*, 2012).

Moreover, in addition to the local climatic response, LULCC can influence the remote climate by inducing a circulation change (Zhao *et al.*, 2001; Lauwaet *et al.*, 2009; Devaraju *et al.*, 2018). A general circulation model (GCM) simulation study suggests that tropical deforestation causes a weakening of deep tropical convection which triggers the northeastward propagation of a Rossby wave train and alters climate at higher latitudes (Snyder, 2010). A coupled ocean-atmosphere model simulation also showed that Southeast Asian deforestation can induce teleconnections between the tropics and the extra tropics via the excitation of atmospheric waves (Schneck and Mosbrugger, 2011). A multi-model inter-comparison study by Pitman *et al.* (2009), as part of the international effort "Land—Use and Climate, Identification of robust impacts" (LUCID), verified the LULCC impact on global climate using seven climate models with a potential map and a specified LULCC map. However, they found disagreement between the models in simulating the LULCC effect. The models had a disagreement in simulating the precipitation and temperature response. These differences were attributed to lack of

consistency in implementing LULCC representation in the models. Another study by Lawrence *et al.* (2018) showed that LULCC can modulate the global carbon cycle. All these studies highlight the important role of land surface conditions in regional and global climate simulations. Apart from historical studies, a number of researchers also studied the impact of LULCC in future projections under different representative concentration pathway (RCP) scenarios (Feddema *et al.*, 2005; Quesada *et al.*, 2017; Lawrence *et al.*, 2018) and highlighted the significant role of LULCC in modulating monsoonal rainfall and global temperature.

All these studies demonstrate the importance of LULCC in the climate system. However, most of the earlier LULCC studies are based on hypothetical assumptions or without implementation of interannual variation of the LULCC map (Xue and Shukla, 1993; Xue and Shukla, 1996; Brovkin *et al.*, 1999; Betts, 2001; Fu, 2003; Feddema *et al.*, 2005; Betts *et al.*, 2007; Pitman *et al.*, 2009; Lawrence and Chase, 2010; Niyogi *et al.*, 2018; Huang *et al.*, 2019). In a recent study, Boone *et al.* (2016) used a LULCC map based on historical land use data (Hurtt *et al.*, 2006, 2011) with five GCMs to study the impact of LULCC on West African regional climate. There is an agreement among the models regarding rainfall reduction in degraded areas. Boone *et al.* (2016) found that over degraded areas increased Bowen ratio resulted in less moisture convergence, causing reduction of convective heating rates linked to reduced latent heat flux (LHF) and moisture flux convergence. They also found that the LULCC model simulations are able to capture the southward shift of rainfall peak in the Sahel region when compared to the control (CTL) simulation; however, this study only considered the LULCC between two decades with no interannual variability.

Klein *et al.* (2017), using a regional Weather Research and Forecast (WRF) model, have shown improvements in rainfall prediction of the West African summer monsoon by incorporating the interannual vegetation fraction and LAI data; however, their study did not consider changes in the vegetation category. Similarly, Meng *et al.* (2014), assessing the influence of realistic interannual vegetation incorporation in the WRF model in simulating the climate variables over southeastern Australia, found significant improvement in air temperature simulation when compared to the simulation with climatological vegetation. The Land Use Model Intercomparison Project (LUMIP) (Lawrence *et al.*, 2016), as part of the Coupled Model Intercomparison Project Phase 6 (CMIP6) experimental design, also suggested LULCC simulations with interannual vegetation. Motivated by these studies and the opportunity provided by recently compiled historical land use data (Hurtt

*et al.*, 2006, 2011) as part of the CMIP6, in this study, we have implemented the LULCC map based on the Hurtt *et al.* (2006, 2011) data with interannual variability, which is a more realistic representation of LULCC in the current context of LULCC impact studies. In long-term simulations, specifying land surface conditions without interannual variations may lead to unrealistic LULCC effect assessment. By adopting realistic LULCC data with interannual variability into an AGCM, this article assesses the impact of LULCC, identifies processes that control the interaction between land surface processes and climate, and evaluates the sensitivity of seasonal variability of rainfall and surface temperature to LULCC. This article is organized as follows: model description and experimental design and methodologies are summarized in Section 2; results are discussed in Section 3; and the conclusions are presented in Section 4.

## 2 | MODEL DESCRIPTION, EXPERIMENTAL DESIGN AND METHODOLOGY

In this study, we have adopted the National Centre for Environmental Prediction (NCEP) Global Forecast System (GFS) (Kalnay *et al.*, 1990; Kanamitsu *et al.*, 1991) model as an AGCM. The NCEP GFS model includes the Moorthi and Suarez (1992) convection scheme, the Chou (1992) and Chou and Suarez (1994) radiation scheme and the Hong and Pan (1996) non-local planetary boundary layer scheme. We set the spectral discretization of the NCEP GFS model at T62L28, which has about 200 km of grid spacing with 28 vertical levels. The NCEP GFS model is coupled with the second version of the Simplified Simple Biosphere land surface model (SSiB2). The SSiB2 is a state-of-the-art vegetation biophysical model that includes photosynthesis in land surface processes while preserving energy, water and momentum conservation at the atmosphere–land surface interface (Xue *et al.*, 1991; Zhan *et al.*, 2003). This model is used for operational forecasting at NCEP and has been extensively validated by NCEP and other researchers around the world (Yuan *et al.*, 2011; Peng *et al.*, 2013; Saha *et al.*, 2014; Ramu *et al.*, 2016; Pillai *et al.*, 2017). In our previous studies this model performance was extensively validated for East Asian monsoon (Xue *et al.*, 2004), South American monsoon (Xue *et al.*, 2006), and global precipitation over many regions (Xue, De Sales, Vasic, *et al.*, 2010). This model also validated in the West African Monsoon Modeling and Evaluation (WAMME) project first and second model intercomparison experiments (Xue, De Sales, Lau, *et al.*, 2010; Xue *et al.*, 2016). Because of these and other (Xue *et al.*, 2004, 2006; Xue, De Sales,

Vasic, *et al.*, 2010; Lee *et al.*, 2018; Huang *et al.*, 2019) evaluation studies, we do not emphasize model performance validation in this study.

LULCC is a gradual change with significant effect on regional and global weather and climate. As mentioned earlier, previous modelling studies implemented LULCC without gradual change, which may lead to unrealistic assessment of LULCC effect. In this study, we have implemented LULCC gradually (potential vegetation map updated annually) to assess the merits of this methodology. We have conducted two experiments, one with a potential vegetation map (Figure 1a; only one potential vegetation map used for the entire simulation) without interannual variability (hereafter referred to as CTL experiment) and another one with an annually varying vegetation map (hereafter referred to as LULCC experiment). In the LULCC experiment, the potential vegetation map is updated annually based on historical land use land cover re-constructed data. Figure 1b shows a snapshot of degraded areas in the year 2010 when compared to the potential vegetation map. As part of the CMIP6 Land Use Model Intercomparison Project

(LUMIP), Hurtt *et al.* (2006, 2011) generated LULCC datasets with the aim of addressing the effects of LULCC on climate, biogeochemical cycling (past–future), and land management strategies to help mitigate climate change. Hurtt *et al.* (2006, 2011) produced the LULCC datasets using multiple models and other estimation data sets such as wood harvest statistics, potential biomass rate, and so on, as inputs. The uncertainty in these inputs affects the quality of the datasets; in particular, assumptions and inherent errors/uncertainties from other models (e.g. the HYDE, Miami-LU ecosystem model) may affect the quality of the datasets. More details can be found in Hurtt *et al.* (2006, 2011). The LULCC data sets are available annually for the time period 850–2,100; in this study, data from 1948 to 2010 are used to create the LULCC vegetation map.

During the period of the study data (1948–2010), there have been significant increases in pasture and croplands globally (Figure 1c) except for over the Eastern United States and Western Europe where there is a clear decrease in the amount of land devoted to crops or pastures. Distinguishing between pasture and crops is

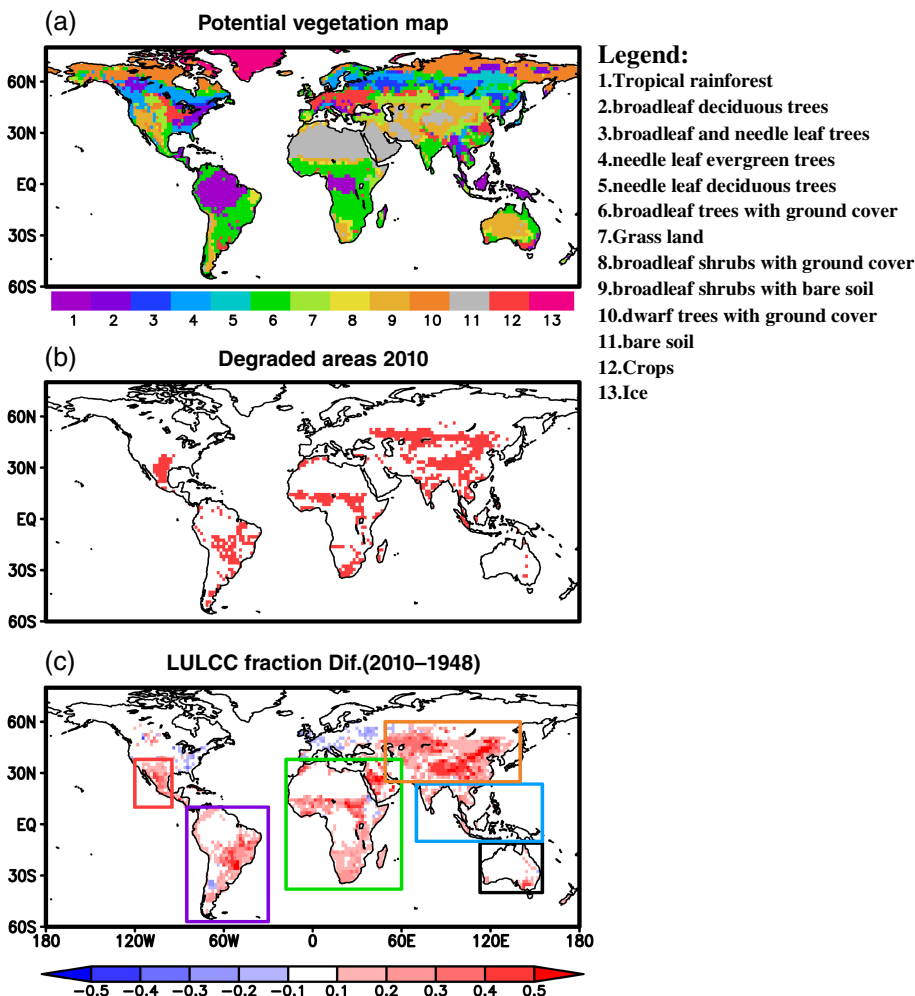


**FIGURE 1** Potential vegetation map used in this study (a), degraded areas in the year 2010 in the LULCC experiment (b) and LULCC fraction difference between 1948 and 2010 (c). Rectangular boxes in upper panel denote the regions used to verify the degradation areas in Figure 2 [Colour figure can be viewed at [wileyonlinelibrary.com](http://wileyonlinelibrary.com)]

difficult, since in reality farmers let their animals graze on croplands after the harvest. Therefore, we have added crops and pastures together to obtain an estimate of the total land cover change. The combined change in crop and pasture fraction relative to the year of 1948 are considered as a LULCC fraction. A methodology was developed to convert Hurtt's LULCC fraction map with  $1^\circ$  resolution to the GCM grid points. In this methodology, total crop and pasture fraction (referred to as LULCC fraction) are calculated at each model grid point from Hurtt's data. Once the LULCC fraction exceeds a threshold value of 75% or increases to 25% relative to the 1948 value, the area (model grid) is specified as degraded in the original GFS-SSiB2 potential vegetation map (see Figure 1a), which is referred to as the CTL run in this article. Based on these criteria we have updated the potential vegetation map annually in the LULCC experiment. Every year at each grid point, if the LULCC fraction value satisfies the above mentioned criteria, those grid's original vegetation is replaced (vegetation classes 1–6 in Figure 1a) with low vegetation (vegetation class 9), while we replace (degraded) low vegetation (vegetation class 7 to 10 from Figure 1a) with bare soil (land use class 11). Other land surface types such as bare soil, crops, and ice were unaltered in the LULCC experiment.

Since the model grid point can only be assigned one vegetation type, we can assign a grid point only with or without land cover change no fractional change is allowed. Our strategy is to ensure the consistency of the trends of the original LULCC fraction change and the trends of change of the fraction of model grid points over different regions in the AGCM LULCC map. Comprehensive evaluations were conducted to make sure the thresholds as

discussed in the previous paragraph were properly assigned. Figure 2 shows the fraction of LULCC in Hurtt's data and the number of degraded/replaced points in the vegetation map in each region. As the amount of degradation LULCC fraction in Hurtt's data increases in each region, the degraded grids in the AGCM potential vegetation map increase accordingly, and there is a large degradation over Euro-Asia and Africa because of intense agricultural activity. Because the entire Mexico region was degraded during 1950 to 1960, the number of degraded grids over that region cannot be increased afterwards. Australia experienced a significant amount of degradation during 1960 to 1980; the degradation area then is substantially reduced after 1980. The black line in Figure 2 denotes the LULCC variability over Australia and shows such a LULCC trend there. It is observed that there is no further increase in land degradation globally after the year 2000. In this study, we only focused on human induced (anthropogenic) LULCCs and their effect on regional and global climate.

By replacing plant function types (PFTs), a set of surface parameters including leaf area index (LAI; Figure 3), short wave reflectance and transmittance on plant leaf surface, greenness, fractional coverage, vegetation height, displacement height, roughness length, soil parameters and all other parameters associated with vegetation are changed to show the degradation effects (Figure 3). Albedo, which is simulated by the SSiB2 based on vegetation conditions, significantly increased in degraded areas (Figure 3) in all seasons because reflection of grass or bare soil is greater than that of tall trees. The model simulations start from January 1948 and are integrated for 63 years to 2010. Two experiments (LULCC and control,

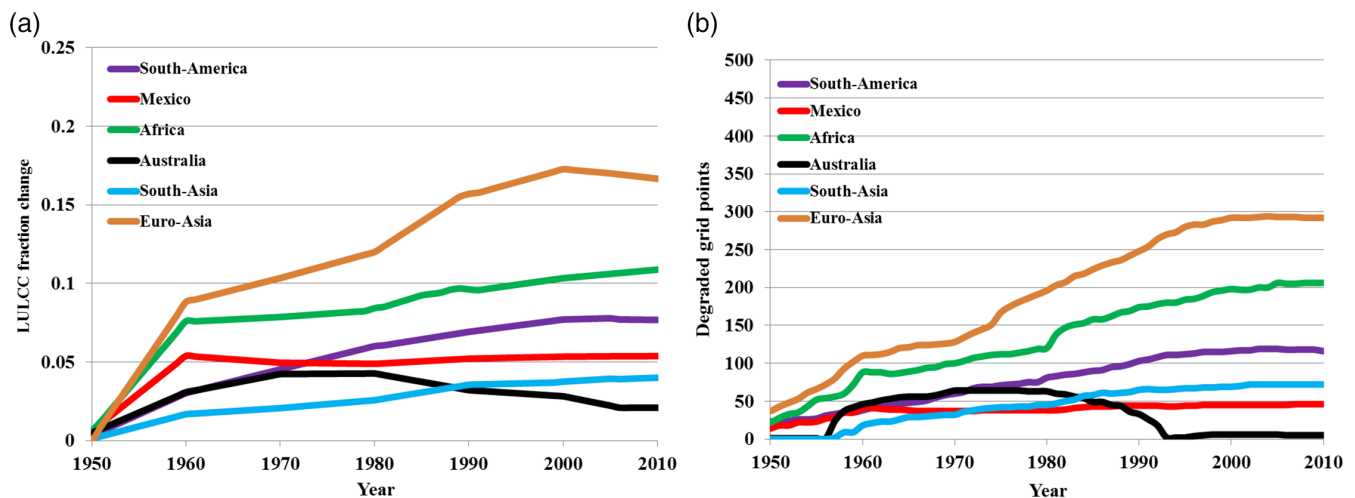


**FIGURE 2** Time series of LULCC fraction difference (left panel) relative to the 1948 for each area specified in the Figure 1 and changes in the number of grid points degraded in each region (right panel) from 1950 to 2010 [Colour figure can be viewed at [wileyonlinelibrary.com](http://wileyonlinelibrary.com)]

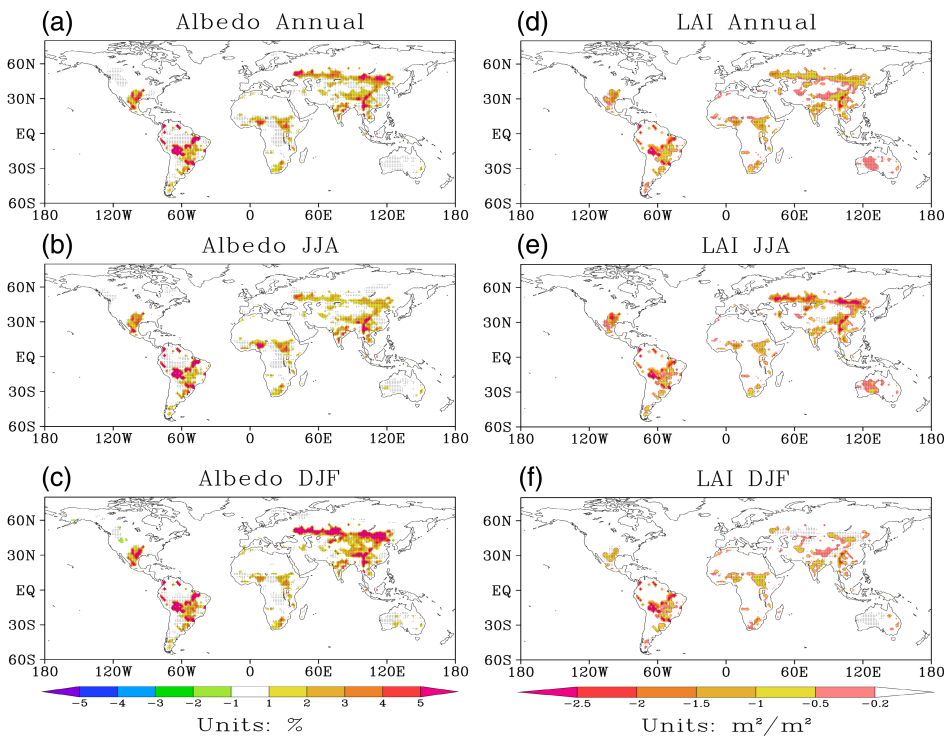


**FIGURE 3** LULCC simulated Albedo difference (%; left column) and leaf area index (LAI) ( $\text{m}^2/\text{m}^2$ ) difference (LULCC – CTL; right column) for annual, JJA and DJF seasons averaged from 1948 to 2010. The stippled region in the figure indicates that the anomalies are significant at 95% based on two tailed Student's *t*-test [Colour figure can be viewed at [wileyonlinelibrary.com](http://wileyonlinelibrary.com)]

CTL) were conducted. Each experiment (LULCC and CTL) has four simulations, and an ensemble mean from these simulations is discussed in the results to reduce model uncertainty. The boundary conditions and initial conditions, including sea surface temperature (SST) and sea ice extent data, are from NCEP reanalysis 1. NCEP Reanalysis datasets were provided by the NOAA/OAR/ESRL PSD, Boulder, CO, and obtained from their web site at <https://www.esrl.noaa.gov/psd/>. To validate the rainfall simulation, the  $1^\circ \times 1^\circ$  observed rainfall dataset from GTS (Chen *et al.*, 2002) and the LST dataset from Climate Research Unit (CRU; Harris *et al.*, 2014) are used.

### 3 | RESULTS

We have evaluated the prescribed LULCC simulation with respect to the control (CTL) simulation in both hydrological cycle and energy balance. Apart from the impact analysis, surface temperature and precipitation simulations are compared with observations to assess the merits of interannual LULCC map representation in the model. In this study, we focused on the LULCC impact over land regions and found that the impact of LULCC was largest during the peak monsoon months. As such, the regional analysis emphasis will be on the respective summer season for each hemisphere. Climate sensitivity over monsoon regions such as East Asia, West Africa and South America (domains are defined in Table S1) is

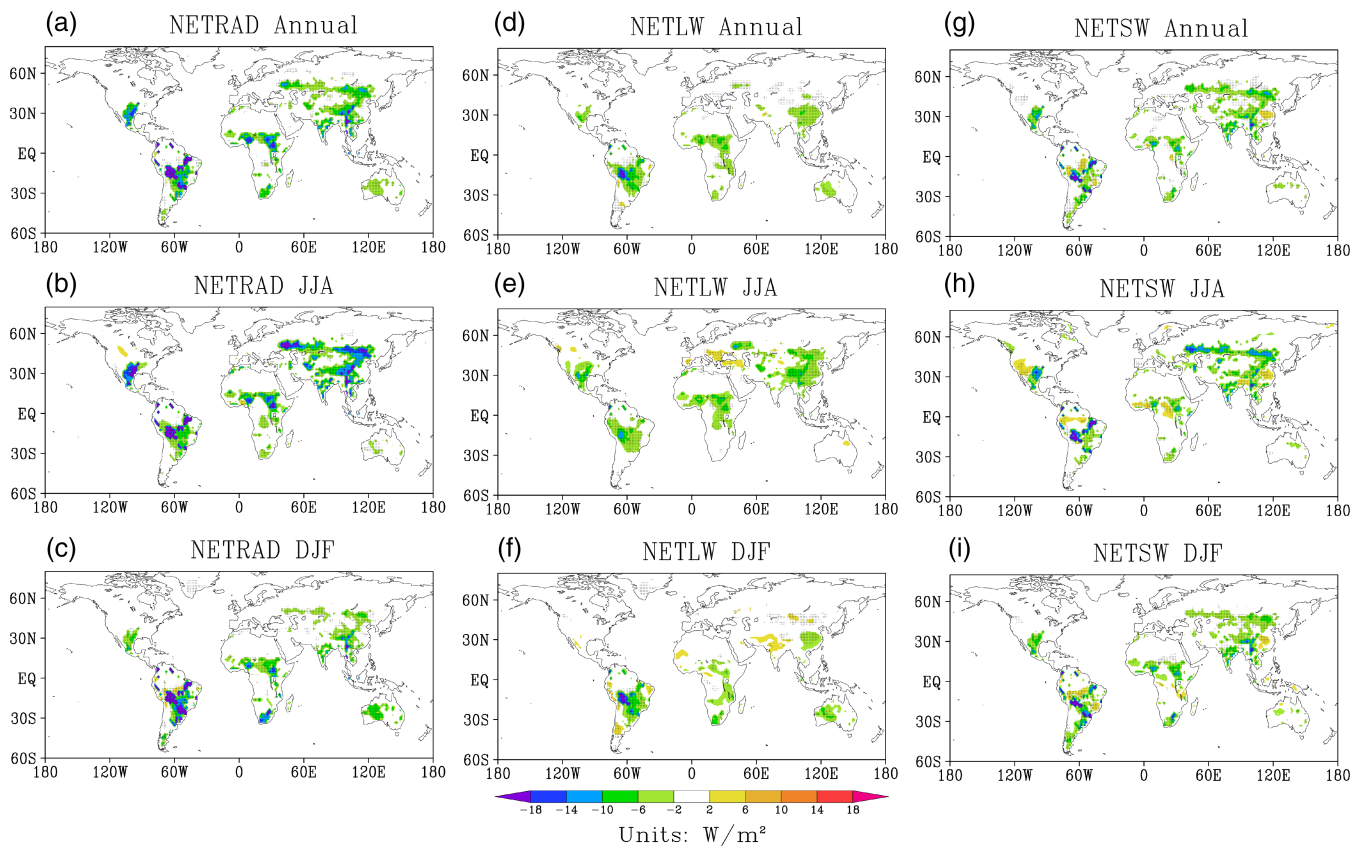
highlighted in the article for better understanding of the LULCC impact and mechanisms. A two-tailed Student's *t*-test is adopted to test for significance of the results presented in this study.

#### 3.1 | Impact of LULCC on surface energy balance and temperature

The land surface conditions play a pivotal role in partitioning of available surface energy between sensible heat and latent heat and the partitioning of water between evaporation and runoff. Any changes in the land surface condition can significantly alter the LAI, albedo, surface roughness, vegetation coverage, greenness, and then surface fluxes. LAI is decreased and albedo significantly increased in all seasons over the degraded areas (Figure 3). The global mean albedo difference between the degradation (LULCC experiment) run and the control run was about 3% over the degraded area (Table 1). The increased albedo caused the reduction in net shortwave radiation (Figure 4g–i) and thereby decreased the net radiation (Figure 4a–c). Net longwave radiation also decreased in all seasons with peak decrease in summer (Figures 4d–f) due to less cloud cover and high surface temperature. The total net radiation decreased more than  $10 \text{ W}/\text{m}^2$  over the degraded areas in all seasons with peak decrease in the summer season (Figure 4b). The variation in surface radiation affected the partitioning of surface fluxes, surface temperature and other associated land

**TABLE 1** Annual mean surface variables and their difference between LULCC and CTL averaged from 1948 to 2010 over global land

	Variable name	Units	Mean (CTL simulation)	Diff (LULCC – CTL)
Annual	Albedo	%	27.66	3.24
	Leaf area index	m <sup>2</sup> /m <sup>2</sup>	2.12	–1.0
	Net surf. radiation	W/m <sup>2</sup>	93.68	–10.9
	Latent heat	W/m <sup>2</sup>	47.38	–8.91
	Sensible heat	W/m <sup>2</sup>	39.92	–2.11
	Ground heat	W/m <sup>2</sup>	0.48	0.12
	Surf. temperature	K	289.78	0.44
	Precipitation	mm/day	2.76	–0.32

**FIGURE 4** LULCC simulated net radiation (left column), net longwave radiation (middle column) and net shortwave radiation (right column) differences (LULCC – CTL) for annual, JJA and DJF season averaged from 1948 to 2010. Units are in W/m<sup>2</sup> for all variables. The stippled region in the figure indicates that the anomalies are significant at 95% based on two tailed Student's *t*-test [Colour figure can be viewed at [wileyonlinelibrary.com](http://wileyonlinelibrary.com)]

variables. The LHF decreased more than 9 W/m<sup>2</sup> over the degraded areas (Figure 5) during the summer season, which can be attributed to the decrease in net radiation and LAI. The reduced LAI, surface roughness, vegetation coverage and greenness in the LULCC experiment resulted in two direct impacts on the surface energy balance. First, albedo over degraded areas increased throughout the whole year with similar magnitude for each season (Figure 3), leading to more shortwave

radiation back into space and a decrease in net radiation fluxes absorbed by the land surface. Meanwhile, decreased roughness length and other vegetation conditions after land degradation reduced the efficiency of momentum transport and latent heat transport from the surface to the atmosphere, resulting in more heat stored at the surface. Reduction in LAI led to the decrease of canopy interception loss and transpiration from the surface. The sensible heat flux (SHF) increased over East



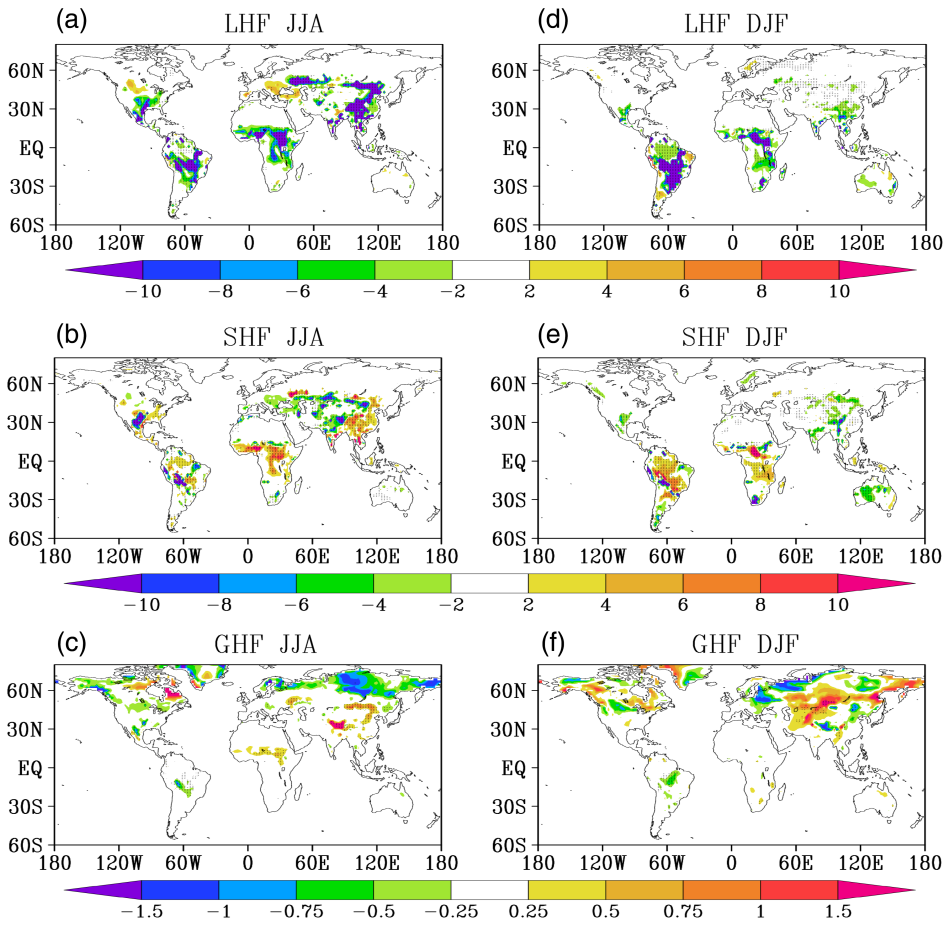


**FIGURE 5** Latent heat flux (LHF), sensible heat flux (SHF) and ground heat flux (GHF) differences (LULCC – CTL) for JJA (left column) and DJF (right column) season averaged from the 1948 to 2010. Units are in  $W/m^2$  for all variables. The stippled region in the figure indicates that the anomalies are significant at 95% based on two tailed Student's *t*-test [Colour figure can be viewed at [wileyonlinelibrary.com](http://wileyonlinelibrary.com)]

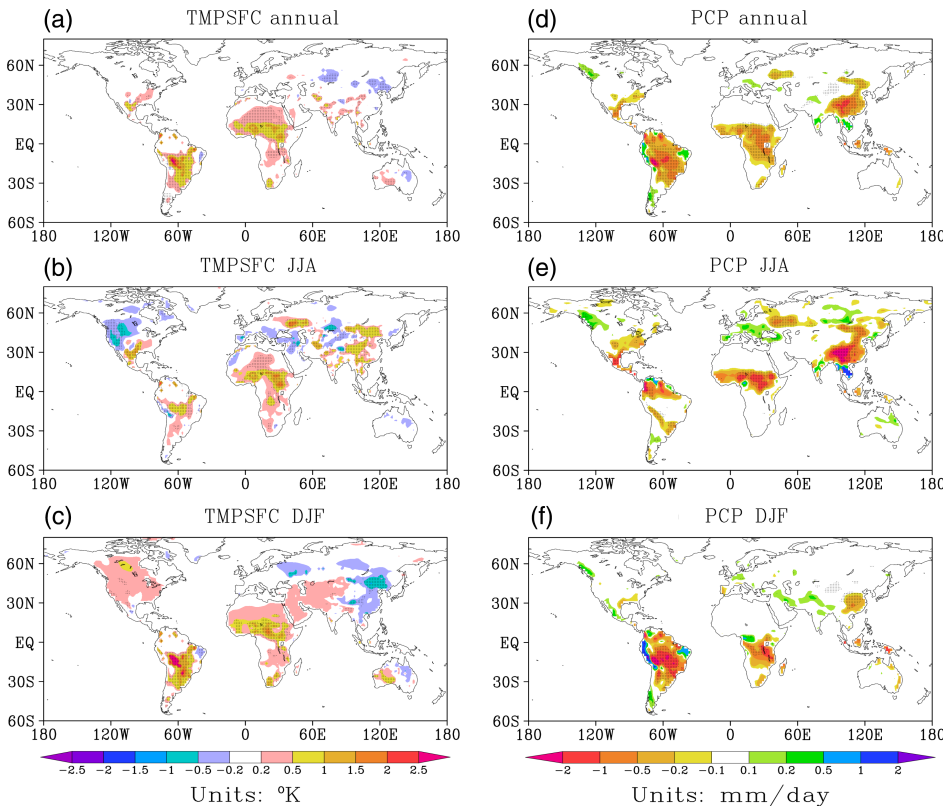


**FIGURE 6** Left column: Surface temperature (K) anomalies (LULCC – CTL) for annual (upper panel), JJA (middle panel) and DJF (lower panel) seasons averaged from 1948 to 2010. Right column: Same as left column but for rainfall anomalies (mm/day). The stippled region in the figure indicate that the anomalies are significant at 95% based on two tailed Student's *t*-test [Colour figure can be viewed at [wileyonlinelibrary.com](http://wileyonlinelibrary.com)]

Asia and West Africa during the boreal summer season (Figure 5) to balance the surface energy budget. Similarly, an increase of SHF was observed over South America and South Africa during austral summer. In these areas, the reduction of LHF was larger than the decrease in net radiation. However, sensible heat decreased in summer over north India, central Asia and a few pockets over Mexico and South America, apparently due to the large albedo increase in those regions. There was an increase in ground heat flux (GHF) over degraded areas (Figure 5).

The LULCC-induced changes in the surface energy balance affect surface temperature. Land degradation led to an annual mean surface temperature warming of 0.44 K and an increase of GHF of 0.12 W/m<sup>2</sup> (Figure 5; Table 1) over degraded areas. Over global land the warming effect was dominant, although there were some regions with a colder surface temperature, such as in

central Asia (Figure 6). The spatial pattern of warming was widespread over large parts of the global land with the strongest signals over degraded areas (Figure 6). The annual warming signal in some regions was substantial, especially over South America and West Africa.

Over degraded areas in East Asia, LULCC caused a strong summer warming of 0.56 K and a winter cooling of 0.32 K. In winter, an increase in albedo by 3% led to a net surface radiation flux decrease, of which 50% was balanced by reduced LHF. In summer, a similar increase in albedo led to a net surface radiation flux decrease of ~13 W/m<sup>2</sup>. However, the decrease in vegetation caused a larger decrease in LHF, ~17 W/m<sup>2</sup>, which outweighs the albedo cooling effect, leading to an increase in GHF (0.25 W/m<sup>2</sup>) and warmer surface temperature. Over degraded area in West Africa, LULCC caused a strong surface warming of 0.82 K during summer (JJA) when compared to the control (CTL) simulation, resulting from a decrease in the net surface

**TABLE 2** Seasonal mean of surface variables and their difference between LULCC and CTL averaged from 1948 to 2010 for various regions

Region	Variable	Mean (CTL simulation)		Diff (LULCC – CTL)	
		JJA	DJF	JJA	DJF
East Asia	Albedo (%)	24.93	28.45	3.01	3.02
	Leaf area index (m <sup>2</sup> /m <sup>2</sup> )	2.82	1.71	-1.14	-0.51
	Net surf. radiation (W/m <sup>2</sup> )	148.92	33.39	-12.8	-5.18
	Latent heat (W/m <sup>2</sup> )	102.57	22.91	-16.71	-2.89
	Sensible heat (W/m <sup>2</sup> )	43.15	7.99	3.66	-2.5
	Ground heat (W/m <sup>2</sup> )	1.6	-0.14	0.25	0.21
	Surf. temperature (K)	295.03	272.02	0.56	-0.32
	Precipitation (mm/day)	8.83	1.08	-1.11	-0.16
West Africa	Albedo (%)	27.66	28.99	2.11	1.36
	Leaf area index (m <sup>2</sup> /m <sup>2</sup> )	1.15	1.37	-0.47	-0.46
	Net surf. radiation (W/m <sup>2</sup> )	120.23	59.52	-7.64	-5.35
	Latent heat (W/m <sup>2</sup> )	51.23	15.53	-10.33	-3.06
	Sensible heat (W/m <sup>2</sup> )	72.53	43.84	2.46	-2.17
	Ground heat (W/m <sup>2</sup> )	-3.27	0.39	0.23	-0.12
	Surf. temperature (K)	302.82	296.31	0.82	0.71
	Precipitation (mm/day)	3.69	0	-0.72	0
South America	Albedo (%)	22.2	21.51	5.58	5.78
	Leaf area index (m <sup>2</sup> /m <sup>2</sup> )	3.28	3.31	-1.63	-1.83
	Net surf. radiation (W/m <sup>2</sup> )	92.06	171.56	-17.01	-24.23
	Latent heat (W/m <sup>2</sup> )	43.51	93.34	-11.21	-21.56
	Sensible heat (W/m <sup>2</sup> )	42.34	58.84	-5.62	-2.61
	Ground heat (W/m <sup>2</sup> )	0.82	-0.84	-0.18	-0.06
	Surf. temperature (K)	293.22	298.36	0.34	1.61
	Precipitation (mm/day)	0.7	6.48	-0.13	-1.2

radiation caused by albedo increase and a larger magnitude of decrease in LHF, which led to an increase in the GHF,  $0.23 \text{ W/m}^2$ , in summer. Over degraded area in South America, which was close to the tropics, LULCC showed a strong summer warming of  $1.61 \text{ K}$  (Table 2). The similar warming patterns are also found in the spring and fall (figure not shown). The increase in albedo caused a net radiation flux decrease of  $24.23 \text{ W/m}^2$  in summer. Both LHF and SHF were reduced. Although the GHF did not change much in the summer, the strong warming effect resulted in a dramatic GHF increase of  $0.93 \text{ W/m}^2$  in the spring season. The heat stored in the thick soil layer of the Amazon during the summer season was slowly released during the spring

season. These results were consistent with similar analysis conducted by Song (2013) for the recent period of 1980–2009.

As discussed earlier, decrease in canopy interception loss and transpiration dominated the change in energy budget and caused warmer temperatures, as shown in Figures 6a–c for the respective summer season in each region. The increasing temperature trends were stronger over East Asia and South America (Figures 7a–d) in the summer season. It should be pointed out that our previous study Kang *et al.* (2007) has shown that by introducing realistic LAI in the GFS, there was significant improvement in surface air temperature and rainfall over

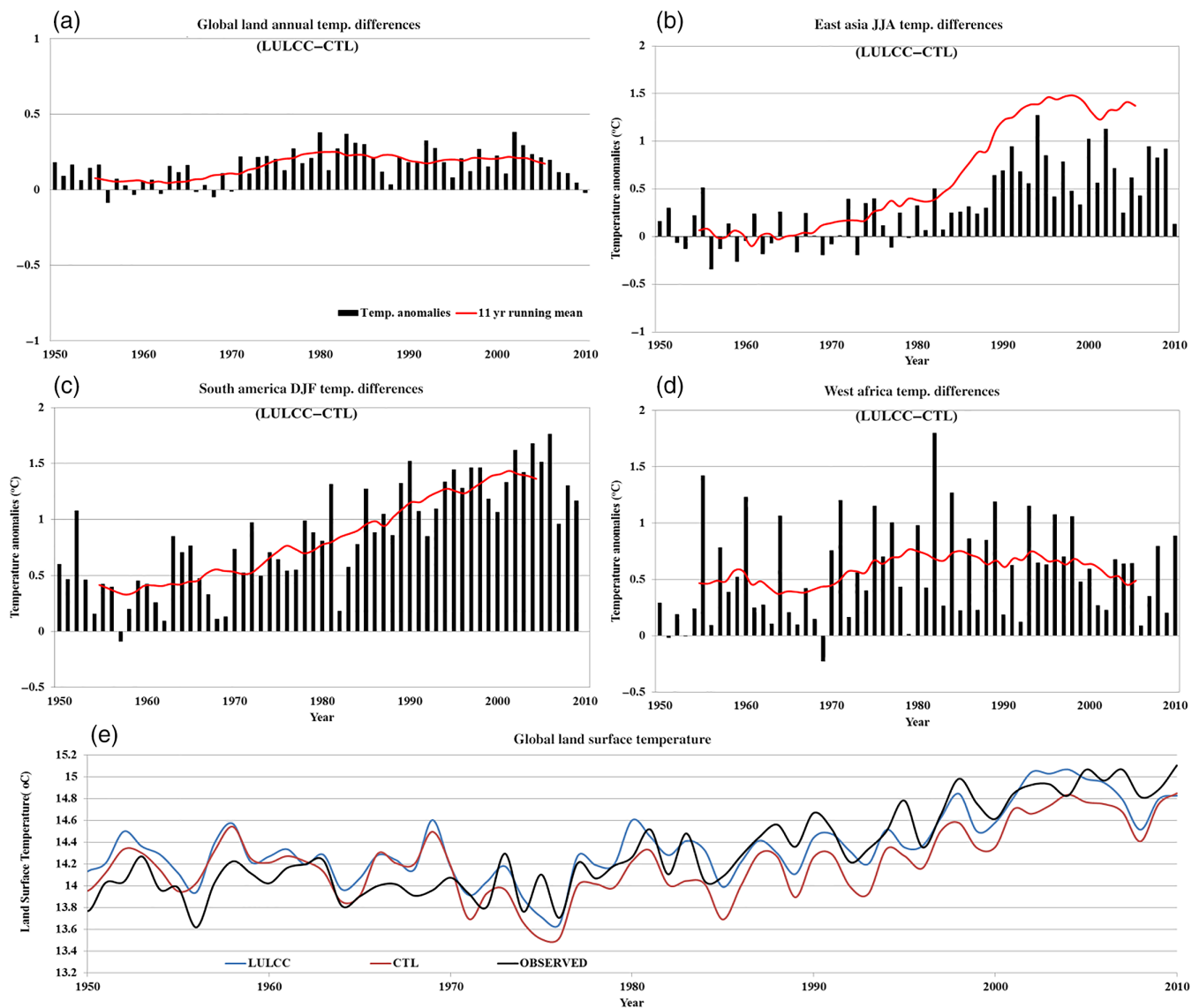
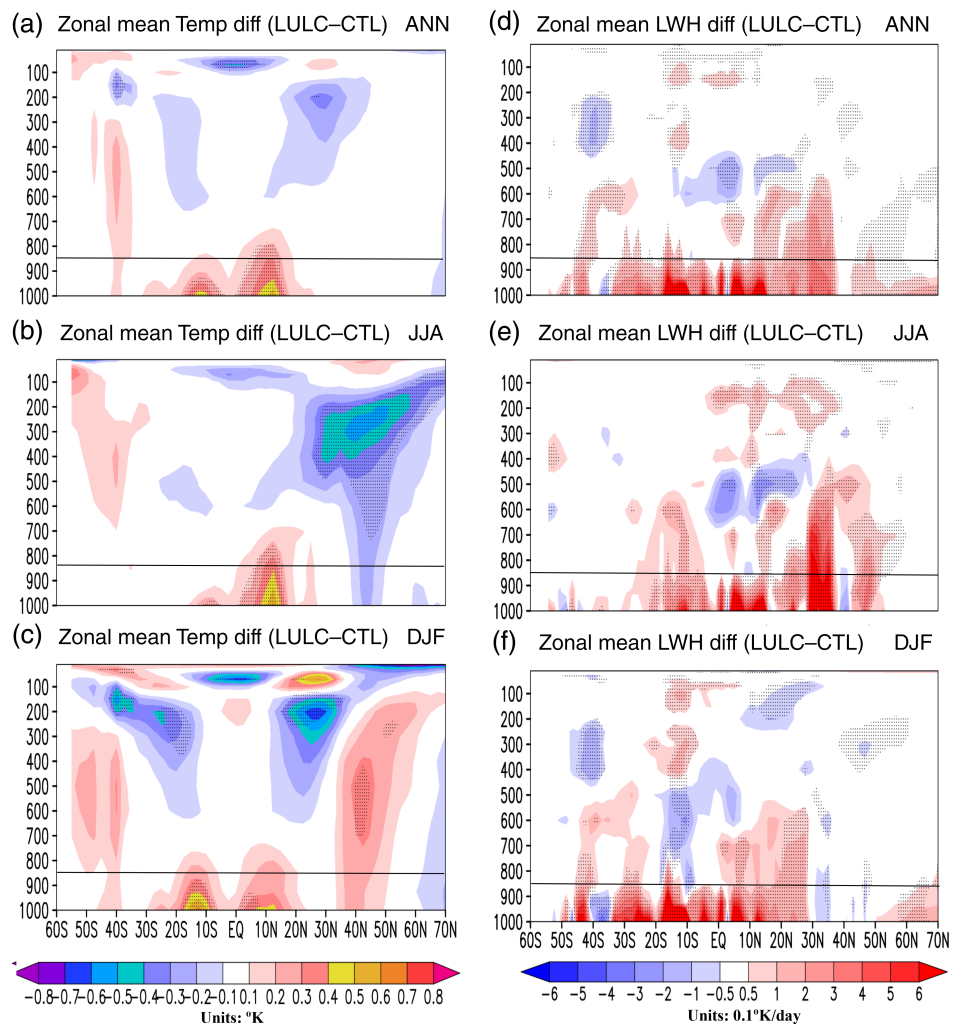


**FIGURE 7** Annual global land mean surface temperature difference (LULCC – CTL) (a); the summer surface temperature difference (LULCC – CTL) over East Asia (b), South America (c), West Africa (d), respectively. The red line in the figures a–d denotes 11 year running mean of anomalies. The comparison of global annual land surface temperature simulation with observation (e) [Colour figure can be viewed at [wileyonlinelibrary.com](http://wileyonlinelibrary.com)]

**TABLE 3** Comparisons of annual mean surface temperature (K) from 1948 to 2010 between CRU data and simulations over different regions

	Region	CTL correlation ( <i>R</i> )	$\Delta R$ (LULCC – CTL)	CTL RMSE ( $\sigma$ )	$\Delta\sigma$ (LULCC – CTL)
Annual	Global Land	.77	.06	0.27	–0.06
	East Asia	.29	.18	0.86	–0.01
	West Africa	.58	.07	0.59	0.06
	South America	.65	.11	1.08	–0.49

**FIGURE 8** Left column: Zonal mean of temperature (K) anomalies (LULCC – CTL) for annual (upper panel), JJA (middle panel) and DJF (lower panel) seasons averaged from 1948 to 2010. Right column: Same as left column but for long wave heating rate (0.1 K/day) anomalies. The stippled region in the figure indicate that the anomalies are significant at 95% based on two tailed Student’s *t*-test. The black horizontal line represents the 850 hPa level [Colour figure can be viewed at [wileyonlinelibrary.com](http://wileyonlinelibrary.com)]



East Asia, North America and West Africa. In this study, with more realistic LULCC data, the LULCC simulation shows significant improvement in interannual temperature prediction when compared to the CTL simulation (Figure 7e). We have compared the temperature simulations with observations over the globe and several regions and found a decrease in temperature biases in the LULCC simulation. Table 3 shows the statistics of the simulated annual mean LST

compared with CRU (Harris *et al.*, 2014) observations from 1948 to 2010. The LULCC simulation improves the correlation coefficients over global land and several sub monsoon domains. The spatial correlation coefficient was increased from 0.29 to 0.47 over East Asia. Although imposing LULCC increased the root mean square error (RMSE) over West Africa by about 10%, it decreased RMSE dramatically (46%) over South America. This improvement suggests that

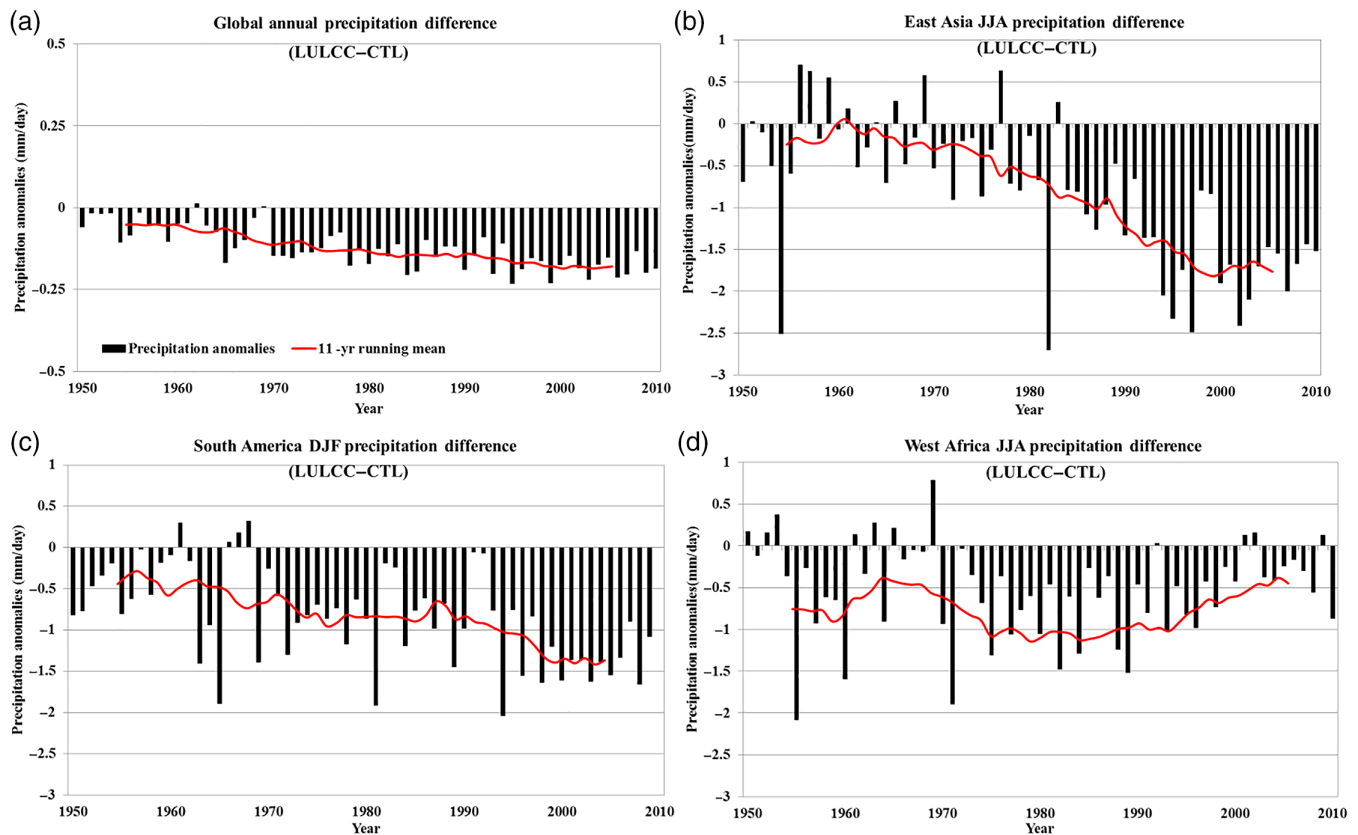


**FIGURE 9** Annual global land mean precipitation difference (mm/day) between LULC and CTL (a); the summer precipitation difference (LULCC – CTL) over East Asia (b), South America (c) West Africa (d), respectively. The red line in the figures a–d denotes 11 year running mean of anomalies [Colour figure can be viewed at [wileyonlinelibrary.com](http://wileyonlinelibrary.com)]

LULCC is an important factor in climate prediction and supports our interannual LULCC specification. The magnitude of the annual surface temperature difference (LULCC minus control) over global land increases with the increase in degradation (Figure 7). The increasing trend was stronger in each region's summer (Table 2), with the strongest trend in South America's summer.

Furthermore, we evaluated the column temperature changes in the troposphere. The zonally averaged annual temperature differences (LULCC – CTL) at the lower troposphere (below 800 hPa) show significant warming in the tropics (Figure 8a). The warming effect was reduced with increasing elevation. There was a cooling above the middle and upper troposphere, with the maximum cooling anomalies above 500 hPa (Figure 8a–c). Due to land degradation, evaporation is less in the LULCC simulation when compared to CTL, which has limited the transport of moisture from surface to upper troposphere and led to a decrease in condensation. The reduced condensation in the upper troposphere led to a decrease in convective heating rate. Meanwhile, the longwave radiation emitted from the land surface warmed the overlying atmosphere up to 800 hPa (Figure 8d–f), causing surface warming.

### 3.2 | Impact of LULCC on precipitation

The LULCC simulations show significant reduction in global rainfall in all seasons (Figure 6d–f). Over degraded area, precipitation was substantially reduced. The most notable changes in precipitation over land were in monsoon regions over East Asia, West Africa, Mexico and South America (Figure 6d–f). The monsoon regions have been identified as the areas that are most sensitive to land-atmosphere interactions (Xue, De Sales, Vasic, *et al.*, 2010). To evaluate LULCC impact on the interannual rainfall simulation, we compared the temporal evolution of surface precipitation anomalies (LULCC – CTL) over global land and regional areas from 1950 to 2010 (Figure 9). The LULCC simulations show more realistic interannual variability and have reduced the model wet biases globally and regionally—especially wet biases over East Asia, which again supports the usage of the interannual LULCC map for this study. The magnitude of annual surface precipitation difference increases as degradation increases over global land (Figure 9). The reduction in magnitude is stronger in each region's summer than in other seasons (Table 2).

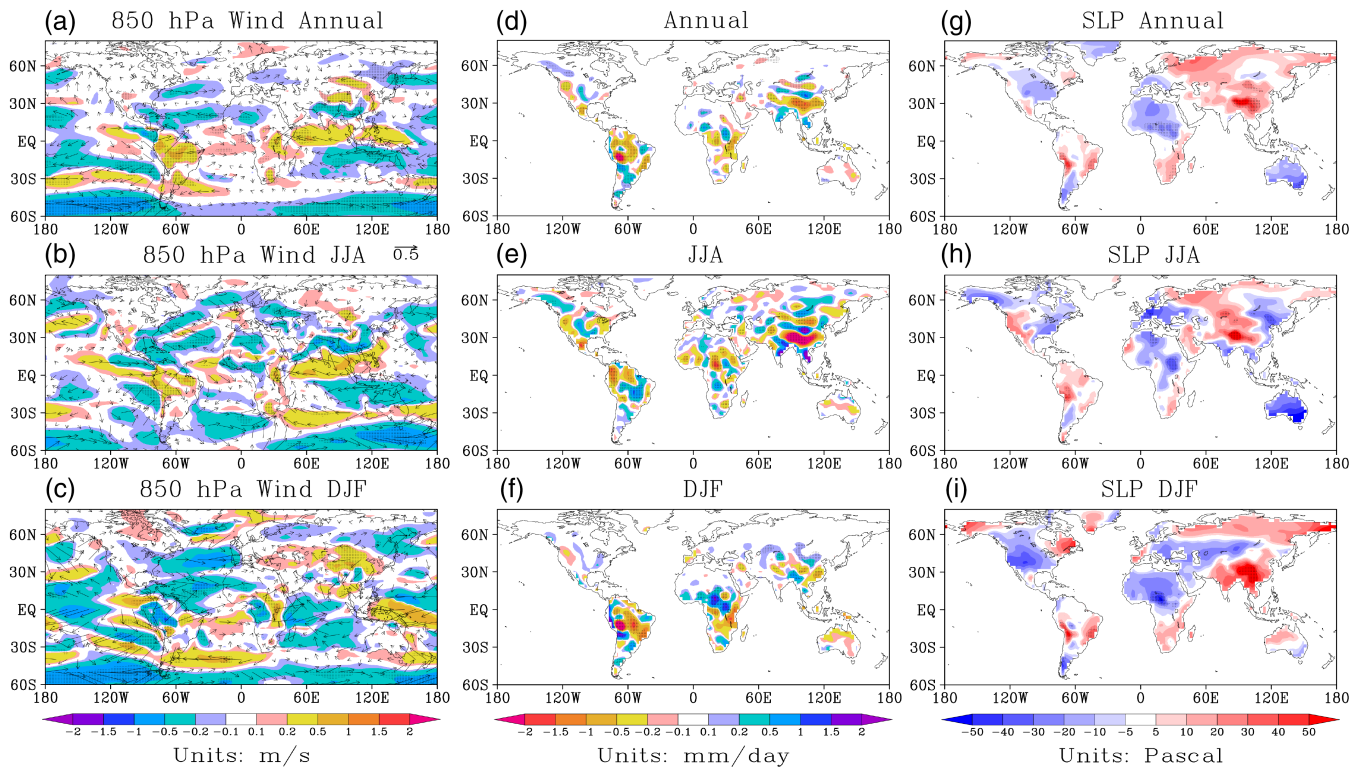


**FIGURE 10** Left column: 850 hPa wind (m/s) anomalies (LULCC – CTL) averaged over the 1948–2010 for annual (upper), JJA (middle) and DJF (lower) seasons. Middle column: Same as left column but for moisture flux convergence (mm/day) anomalies. Right column: Same as left column but for Sea level pressure (Pa) anomalies. The stippled region in the figure indicate that the anomalies are significant at 95% based on two tailed Student's *t*-test [Colour figure can be viewed at [wileyonlinelibrary.com](http://wileyonlinelibrary.com)]

East Asia and South America exhibited increased reduction of precipitation with increasing magnitude of LULCC, and the strongest reduction was in South America's summer. Meanwhile, West Africa shows a strong rainfall reduction from 1950 through 1990 and the dry anomalies were reduced in the recent decade. The expansion of LULCC led to an annual global mean surface precipitation reduction of 0.32 mm/day over degraded area (Table 1). Over Asia during the JJA season, rainfall reduced significantly. Over Southeast China, rainfall reduced nearly 2 mm/day and the Mongolian and surrounding regions experienced significant reduction by about 1 mm/day when compared to the CTL simulation (Figure 6e). Similarly, rainfall also reduced 1–2 mm/day over West Africa, Sudan, Colombia, and Mexico (Figure 6e). During the austral summer season, South America and southern Africa experienced a reduction of rainfall in monsoon regions except Peru and South Argentina, which received slightly increased rainfall compared to the CTL simulation (Figure 6f). The reduction in precipitation is mainly confined within the LULCC regions.

The precipitation reduction in the LULCC experiment is related to the reduction in surface evaporation and

relative moisture flux divergence. The reduction in vegetation (Figure 1) led to a reduction in water released into the atmosphere from the surface through a reduction in transpiration and canopy evaporation. Over West Africa in the summer, the southeasterly airflow from the Indian Ocean, driven by the Indian Ocean high pressure, became southwesterly after crossing the equator in Central Africa and formed the convergence zone over the Sahel, which was relevant to the summer monsoon in that region. In the LULCC experiment, lower surface pressure over the Sahel (Figure 10h) than in the CTL experiment led to a stronger low-level southwest wind. However, the lack of evaporation outweighed the impact of the pressure gradient change, which caused a precipitation reduction over the convergence centre. Over degraded areas, LHF reduced more than 10 W/m<sup>2</sup> in both JJA and DJF (Figure 5) seasons. In addition, moisture transport from the surrounding oceans was also altered by LULCC. In the summer, the low-level southwest airflow brings moisture to Asia, which has a low surface pressure, and a counterclockwise turning circulation is formed. The monsoonal flow (850 hPa wind), which transports moisture to the Asian landmass during the JJA season, is relatively weak (Figure 10b) over north India

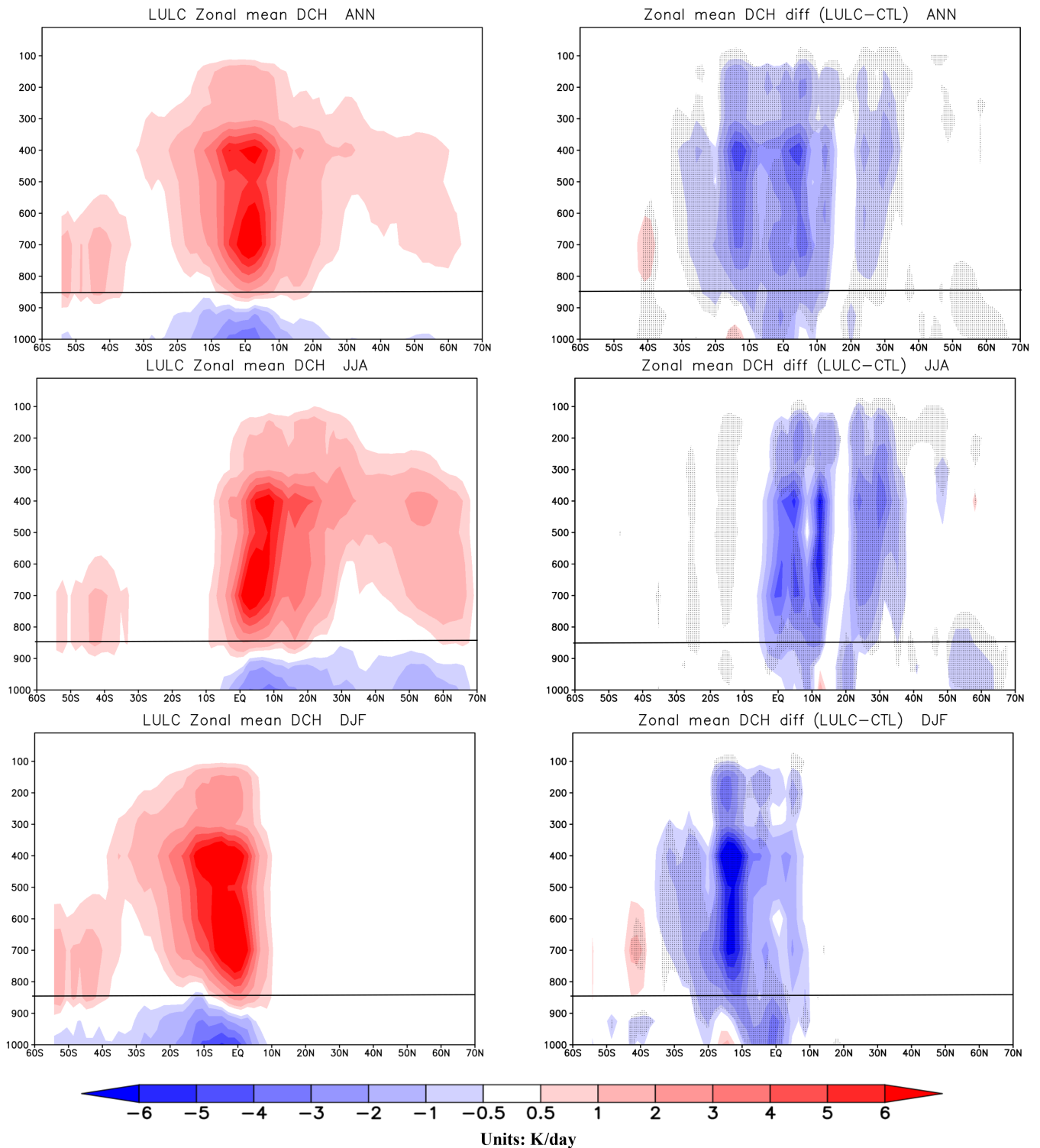


**FIGURE 11** LULCC simulated deep convective heating rate (K/day) seasonal mean (left column) and difference (0.1 K/day, LULCC – CTL; right column) averaged from 1948 to 2010. The stippled region in the figure indicate that the anomalies are significant at 95% based on two tailed Student's *t*-test. The black horizontal line represents the 850 hPa level [Colour figure can be viewed at [wileyonlinelibrary.com](http://wileyonlinelibrary.com)]

and south China in the LULCC simulation. The moisture convergence over south China significantly reduced by about 2 mm/day (Figure 10e), consistent with strong dry

anomalies over that region. The LULCC experiment produced higher surface pressure over East Asia (Figure 10g–i) compared to that simulated in the CTL

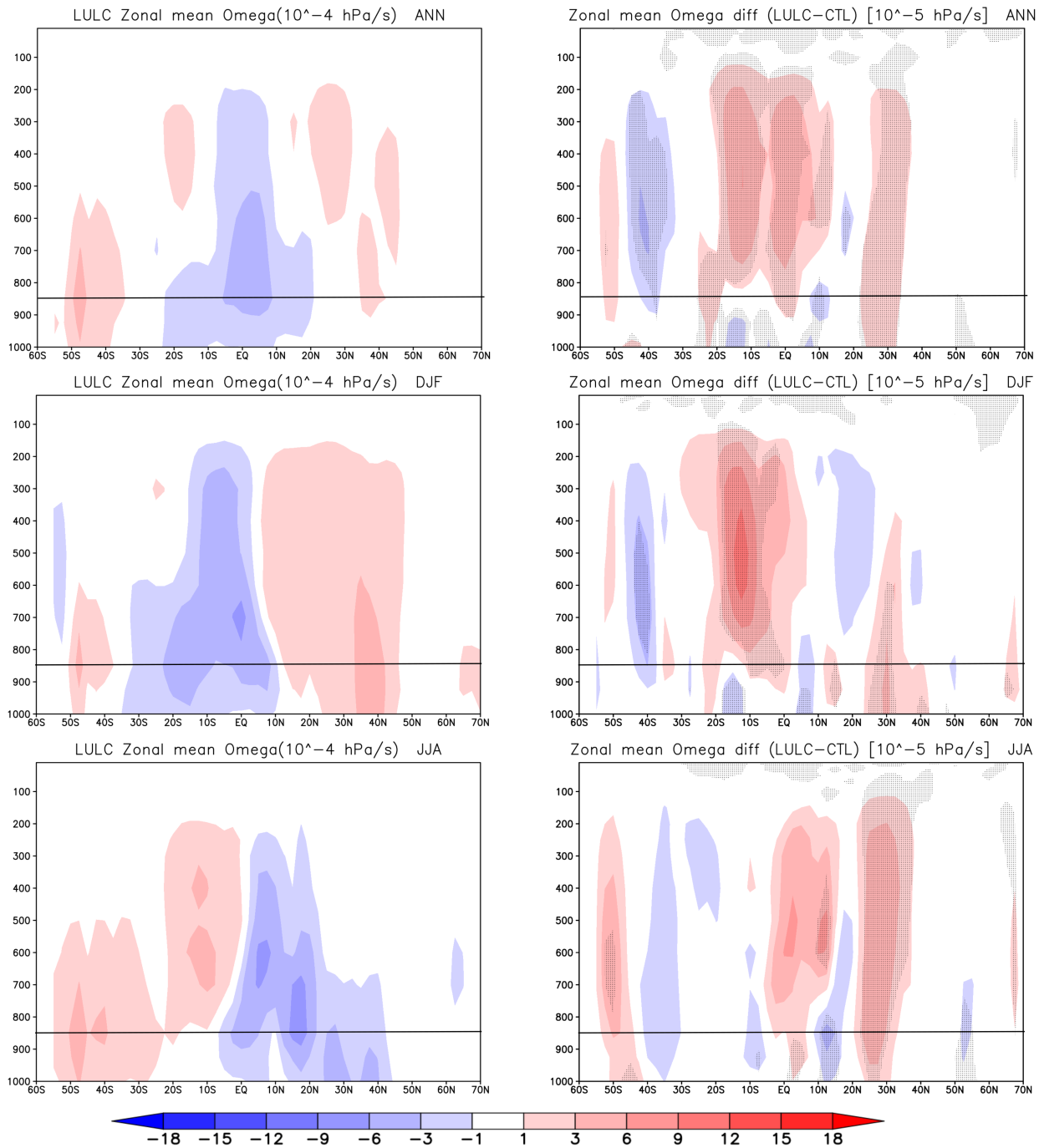


**FIGURE 12** LULCC simulated zonal mean of vertical motion ( $10^{-4}$  hPa/s, left column) and difference ( $10^{-5}$  hPa/s, LULCC – CTL, right column) averaged from 1948 to 2010. The stippled region in the figure indicate that the anomalies are significant at 95% based on two tailed Student’s *t*-test. The black horizontal line represents the 850 hPa level [Colour figure can be viewed at [wileyonlinelibrary.com](http://wileyonlinelibrary.com)]

experiment, which led to a weaker low-level southwest airflow.

To further understand the weakening of circulation over monsoon regions, we analysed the zonal mean of deep convective heating rate throughout the atmospheric column. Deep convective heating rate was reduced in LULCC experiments (Figure 11) when compared to the CTL simulation in all seasons in tropical regions where

convection is dominant from the surface to 200 hPa. The reduction in convective heating rate led to a decrease of tropospheric temperature gradients, which caused weaker wind circulation. Apart from this, we also observed the subsidence of air (Figure 12) in those regions. The subsidence caused increase of surface pressure, and these positive feedbacks led to reduction of rainfall in monsoon dominant regions. The reduction in rainfall over



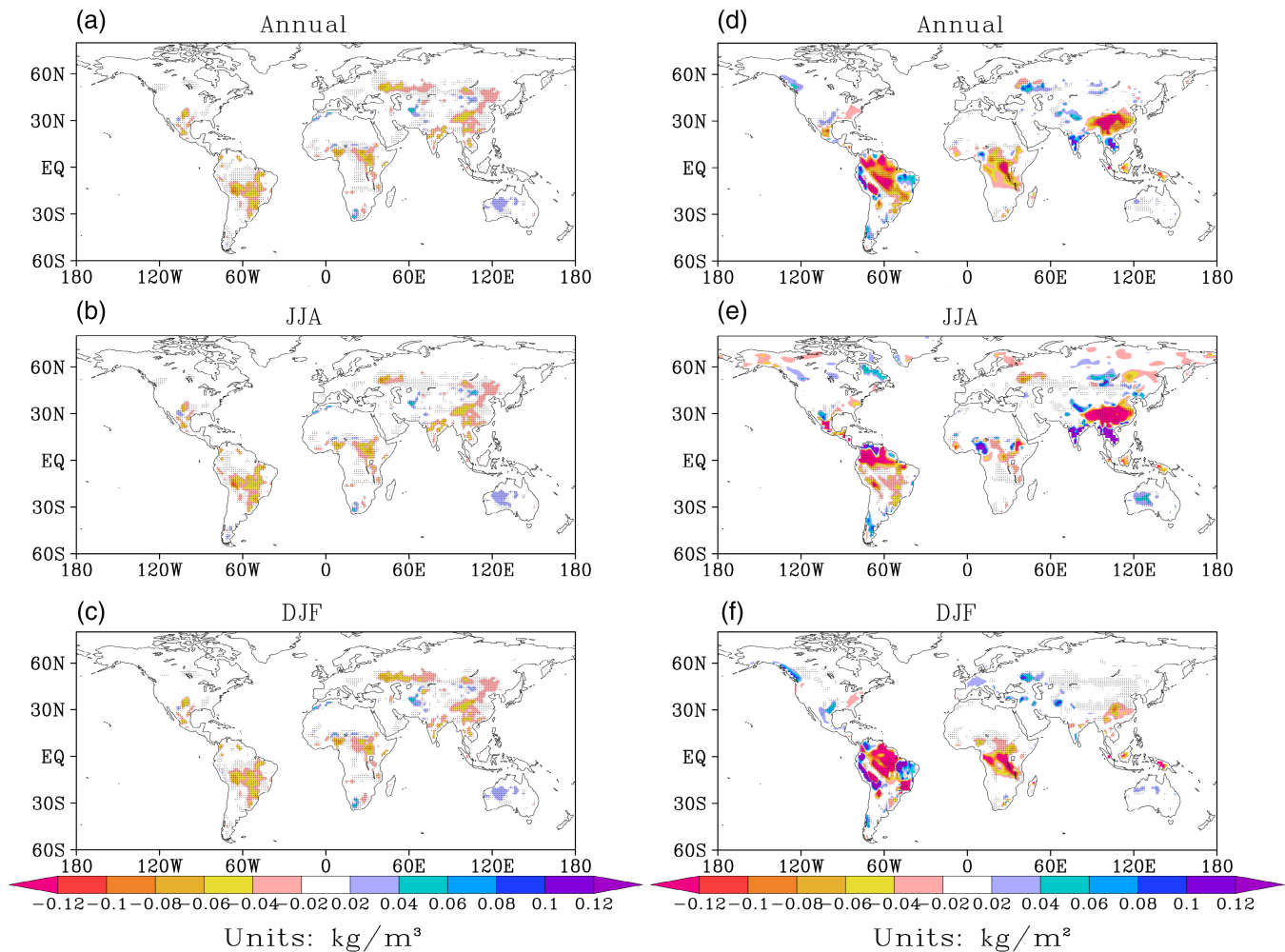


**FIGURE 13** Left column: Second layer (10–40 cm) soil moisture ( $\text{kg}/\text{m}^3$ ) anomalies (LULCC – CTL) averaged over 1948–2010 for annual, JJA and DJF seasons. Right column: same as left column but for surface runoff anomalies (LULCC – CTL;  $\text{kg}/\text{m}^2$ ). The stippled region in the figure indicate that the anomalies are significant at 95% based on two tailed Student's *t*-test [Colour figure can be viewed at [wileyonlinelibrary.com](http://wileyonlinelibrary.com)]

degraded area further led to reduction in soil moisture and runoff in the LULCC simulation (Figure 13). The reduction in soil moisture in degraded areas led to less water evaporation from soil and less moisture availability in those regions and formed a positive feedback.

#### 4 | CONCLUSION

In this study, we have evaluated the impact of LULCC on temperature and precipitation from 1948 to 2010 by specifying LULCC in a GCM with the most recent LULCC data, which has relative realistic interannual variability, instead of specifying one fixed hypothetical LULCC map as in many previous studies (e.g., Xue and Shukla, 1993; Pitman *et al.*, 2009; Boisier *et al.*, 2012). We have degraded (replacing original land use category with another category) the potential vegetation

classification map progressively relative to the vegetation distribution conditions in 1948 based on LULCC fraction data. The simulated results with this LULCC map with interannual variation show improvement in interannual temperature and precipitation variability and reduction in bias, which suggests the role of LULCC in the climate system.

LULCC alters the surface energy balance by modifying albedo, roughness length, and LAI. In the LULCC experiment, changes in vegetation category increased albedo because of decrease in the LAI index, which led to the decrease of net shortwave radiation. Evapotranspiration also reduced because of reduction in vegetation fraction which led to less cloud fraction due to less moisture availability in the atmosphere which led to decrease (by allowing more longwave radiation to escape) in net longwave radiation at the surface. We found that LULCC increased land surface temperatures in tropical regions

primarily due to decrease of evapotranspiration which outweighed the cooling effect of the decrease in net radiation, with peak values in the summer season and cooler surface temperatures at middle and high altitudes where lost convective heating plays a dominant role. At regional scale, the LULCC effect varied with locations and seasons. Over East Asia, during summer (JJA) there was a strong surface warming (0.56 K) and moderate cooling in winter (DJF) because increased albedo dominates the LHF heating effect. LULCC caused significant warming over South America (1.61 K) and Africa in all seasons with peak warming in the respective summer seasons. The results suggest that LULCC could amplify ongoing surface warming (in addition to greenhouse gas warming) over the land degradation regions, which could further warm the surface in the future with increased population and associated agriculture intensification.

Reduction in vegetation and increase in surface albedo in the LULCC experiment caused less evapotranspiration and changes in moisture convergence, which led to precipitation reduction globally, with the strongest signals over the degraded regions. Decrease in evapotranspiration led to less moisture availability in the upper atmosphere, and limited latent heat release in the upper troposphere led to a cooler upper atmosphere, which in turn narrowed the tropospheric temperature gradient, which plays a significant role in transporting the moisture from adjacent sea regions to monsoon regions during the summer season. Convective heating rate significantly reduced in the LULCC experiment when compared to the CTL experiment, which caused weaker wind circulation due to a weaker tropospheric temperature gradient. The subsidence in the degraded areas led to increase of surface pressure and decrease of rainfall in those regions. The reduction in rainfall over degraded area caused further decrease of soil moisture and in turn led to decrease of evaporation and evapotranspiration in that region, forming a positive feedback. Precipitation reduction was strongest in South America (−1.2 mm/day) and East Asia (−1.1 mm/day) due to the largescale degradation over that region. The expansion of LULCC led to an annual mean surface precipitation reduction of −0.32 mm/day over degraded areas. The reduction in rainfall magnitude increased globally with increasing LULCC fraction, and the strongest reduction was in South America's summer.


Due to the coarse resolution of this experiment, it is hard to identify the spatial pattern of temperature and rainfall or the vertical structure of heating rates at regional scales, especially over coastal or mountain regions, in detail. Since the experiment uses specified SST, the ocean feedbacks/responses are missing. Therefore, it is necessary to extend the LULCC study using coupled ocean–atmosphere–land general circulation

models. Apart from this, in the beginning of 21st century many countries adopted the better land use management policies to mitigate the climate change. For instance, the Green for Grain (Hua *et al.*, 2016) is one of the initiative by China's reforestation scheme. Similar programs were adopted by many countries to restore the vegetation (Chen *et al.*, 2019). Most of these program's reforestation effect felt is in recent years when the trees are grown up. Hence, further study is required to comprehensively investigate this reforestation effect by extending the study period to recent years. Furthermore, there are several other issues that need to be addressed in the future LULCC studies. For instance, the photosynthesis process is not included in the SSiB version that is used for this study; therefore, the effect of LULCC on the carbon budget is not included. The model does not include a dynamic vegetation component and aerosol emission, which is also a limitation and produces some uncertainty in assessing the LULCC effect. In addition, the results presented in this study also depend on the quality of the LULCC fraction data produced by Hurtt *et al.* (2006, 2011). Further LULCC studies are necessary to address these issues.

#### ACKNOWLEDGEMENT

The authors would like to acknowledge the research grant AGS-1419526 supported by the United States National Science Foundation (U.S. NSF). We would like to extend our sincere gratitude to the Texas Advanced Computing Center (TACC) at the University of Texas at Austin for providing High-Performance Computing (HPC) resources. Some tests were also conducted using the National Center for Atmospheric Research supercomputer. We would also like to acknowledge Guoqiong Song of UCLA for carrying out the simulations.

#### ORCID

Nagaraju Chilukoti  <https://orcid.org/0000-0002-8806-1646>

#### REFERENCES

- Bamba, A., Diallo, I., Touré, N.E., Kouadio, K., Konaré, A., Dramé, M.S., Diedhiou, A., Silué, S., Doumbia, D and Tall, M. (2018). Effect of the African greenbelt position on West African summer climate: a regional climate modeling study. *Theoretical and Applied Climatology*, 137(1–2), 309–322. <https://doi.org/10.1007/s00704-018-2589-z>.
- Beltrán-Przekurat, A., Pielke, R.A., Eastman, J.L. and Coughenour, M.B. (2012) Modelling the effects of land-use/land-cover changes on the near-surface atmosphere in southern South America. *International Journal of Climatology*, 32, 1206–1225. <https://doi.org/10.1002/joc.2346>.
- Betts, R.A. (2001) Biogeophysical impacts of land use on present-day climate: near-surface temperature change and radiative

- forcing. *Atmospheric Science Letters*, 2, 39–51. <https://doi.org/10.1006/asle.2001.0023>.
- Betts, R.A., Falloon, P.D., Goldewijk, K.K. and Ramankutty, N. (2007) Biogeophysical effects of land use on climate: model simulations of radiative forcing and large-scale temperature change. *Agricultural and Forest Meteorology*, 142, 216–233. <https://doi.org/10.1016/j.agrformet.2006.08.021>.
- Boisier, J.P., de Noblet-Ducoudré, N., Pitman, A.J., Cruz, F.T., Delire, C., van den Hurk, B.J.J.M., M.K. van der Molen, C. Müller, Voltaire, A. (2012). Attributing the impacts of land-cover changes in temperate regions on surface temperature and heat fluxes to specific causes: Results from the first LUCID set of simulations. *Journal of Geophysical Research: Atmospheres*, 117(D12), n/a-n/a. <https://doi.org/10.1029/2011jd017106>.
- Boone, A.A., Xue, Y., De Sales, F., Comer, R.E., Hagos, S., Mahanama, S., Kathleen Schiro, Guoqiong Song, Guiling Wang, S. Li & Carlos R. Mechoso (2016) The regional impact of land-use land-cover change (LULCC) over West Africa from an ensemble of global climate models under the auspices of the WAMME2 project. *Climate Dynamics*, 47, 3547–3573. <https://doi.org/10.1007/s00382-016-3252-y>.
- Borrego, C., Martins, H., Tchepel O., Salmim, L., Monteiro, A., & Miranda, A. I. (2006) How urban structure can affect city sustainability from an air quality perspective. *Environmental Modelling and Software*, 21, 461–467.
- Brovkin, V., Ganopolski, A., Claussen, M., Kubatzki, C. and Petoukhov, V. (1999) Modelling climate response to historical land cover change. *Global Ecology and Biogeography*, 8, 509–517. <https://doi.org/10.1046/j.1365-2699.1999.00169.x>.
- Cárdenas Rodríguez, M., Dupont-Courtade, L. and Oueslati, W. (2016) Air pollution and urban structure linkages: evidence from European cities. *Renewable and Sustainable Energy Reviews*, 53, 1–9. <https://doi.org/10.1787/5jrp6w9xlbq6-en>.
- Chen, C., Park, T., Wang, X., Piao, S., Xu, B., Chaturvedi, R.K., Fuchs, R., Brovkin, V., Ciais, P., Fensholt, R., Tømmervik, H., Bala, G., Zhu, Z., Nemani, R.R. and Myneni, R.B. (2019) China and India lead in greening of the world through land-use management. *Nature Sustainability*, 2, 122–129. <https://doi.org/10.1038/s41893-019-0220-7>.
- Chen, M., Xie, P. and Janowiak, J.E. (2002) Global land precipitation: a 50-yr monthly analysis based on gauge observations. *Journal of Hydrometeorology*, 3, 249–266. [https://doi.org/10.1175/1525-7541\(2002\)003<0249:GLPAYM>2.0.CO;2](https://doi.org/10.1175/1525-7541(2002)003<0249:GLPAYM>2.0.CO;2).
- Cho, H.S. and Choi, M.J. (2014) Effects of compact urban development on air pollution: empirical evidence from Korea. *Sustainability*, 6, 5968–5982. <https://doi.org/10.3390/su6095968>.
- Chou, M.-D. (1992) A solar radiation model for use in climate studies. *Journal of the Atmospheric Sciences*, 49, 762–772. [https://doi.org/10.1175/1520-0469\(1992\)049<0762:asrmfu>2.0.co;2](https://doi.org/10.1175/1520-0469(1992)049<0762:asrmfu>2.0.co;2).
- Chou M-D, Suarez MJ (1994) Technical report series on global modeling and data assimilation. Volume 3: An efficient thermal infrared radiation parameterization for use in general circulation models.
- Clark, D.B., Xue, Y., Harding, R.J. and Valdes, P.J. (2001) Modeling the impact of land surface degradation on the climate of tropical North Africa. *Journal of Climate*, 14, 1809–1822. [https://doi.org/10.1175/1520-0442\(2001\)014<1809:MTIOLS>2.0.CO;2](https://doi.org/10.1175/1520-0442(2001)014<1809:MTIOLS>2.0.CO;2).
- Davin, E.L. and de Noblet-Ducoudre, N. (2010) Climatic impact of global-scale deforestation: Radiative versus nonradiative processes. *Journal of Climate*, 23, 97–112. <https://doi.org/10.1175/2009JCLI3102.1>.
- de Noblet-Ducoudré, N., Boisier, J.P., Pitman, A., Bonan, G.B., Brovkin, V., Cruz, F., Delire, C., Gayler, V., Van den Hurk, B.J. J.M., Lawrence, P.J., Van Der Molen, M.K., Müller, C., Reick, C.H., Strengers, B.J. and Voltaire, A. (2012) Determining robust impacts of land-use-induced land cover changes on surface climate over North America and Eurasia: results from the first set of LUCID experiments. *Journal of Climate*. <https://doi.org/10.1175/JCLI-D-11-00338.1>.
- Devaraju, N., de Noblet-Ducoudré, N., Quesada, B. and Bala, G. (2018) Quantifying the relative importance of direct and indirect biophysical effects of deforestation on surface temperature and teleconnections. *Journal of Climate*, 31, 3811–3829. <https://doi.org/10.1175/JCLI-D-17-0563.1>.
- Duveiller, G., Hooker, J. and Cescatti, A. (2018) The mark of vegetation change on Earth's surface energy balance. *Nature Communications*, 9, 679. <https://doi.org/10.1038/s41467-017-02810-8>.
- Feddema, J.J. (2005). The Importance of Land-Cover Change in Simulating Future Climates. *Science*, 310(5754), 1674–1678. <https://doi.org/10.1126/science.1118160>.
- Fu, C. (2003) Potential impacts of human-induced land cover change on East Asia Monsoon. *Global and Planetary Change*, 37, 219–229.
- Halder, S., Saha, S.K., Dirmeyer, P.A., Chase, T.N. and Goswami, B. N. (2016) Investigating the impact of land-use land-cover change on Indian summer monsoon daily rainfall and temperature during 1951-2005 using a regional climate model. *Hydrology and Earth System Sciences*, 20, 1765–1784. <https://doi.org/10.5194/hess-20-1765-2016>.
- Harris, I., Jones, P.D., Osborn, T.J. and Lister, D.H. (2014) Updated high-resolution grids of monthly climatic observations - the CRU TS3.10 dataset. *International Journal of Climatology*, 34, 623–642. <https://doi.org/10.1002/joc.3711>.
- Hong, S.Y. and Pan, H.L. (1996) Nonlocal boundary layer vertical diffusion in a medium-range forecast model. *Monthly Weather Review*, 124, 2322–2339. [https://doi.org/10.1175/1520-0493\(1996\)124<2322:NBLVDI>2.0.CO;2](https://doi.org/10.1175/1520-0493(1996)124<2322:NBLVDI>2.0.CO;2).
- Hua, F., Wang, X., Zheng, X., Fisher, B., Wang, L., Zhu, J., Tang, Y., Yu, D.W. and Wilcove, D.S. (2016) Opportunities for biodiversity gains under the world's largest reforestation programme. *Nature Communications*, 7, 1–11. <https://doi.org/10.1038/ncomms12717>.
- Huang, H., Gu, Y., Xue, Y., Jiang, J. and Zhao, B. (2019) Assessing aerosol indirect effect on clouds and regional climate of east/South Asia and West Africa using NCEP GFS. *Climate Dynamics*, 52, 5759–5774. <https://doi.org/10.1007/s00382-018-4476-9>.
- Hurt, G.C., Chini, L.P., Frolking, S., Betts, R.A., Feddema, J., Fischer, G., Fisk, J.P., Hibbard, K., Houghton, R.A., Janetos, A., Jones, C.D., Kindermann, G., Kinoshita, T., Klein Goldewijk, K., Riahi, K., Shevliakova, E., Smith, S., Stehfest, E., Thomson, A., Thornton, P., van Vuuren, D.P. and Wang, Y.P. (2011) Harmonization of land-use scenarios for the period 1500-2100: 600 years of global gridded annual land-use transitions, wood harvest, and resulting secondary lands. *Climatic Change*, 109, 117–161. <https://doi.org/10.1007/s10584-011-0153-2>.

- Hurtt, G.C., Frolking, S., Fearon, M.G., et al. (2006) The underpinnings of land-use history: three centuries of global gridded land-use transitions, wood-harvest activity, and resulting secondary lands. *Global Change Biology*, 12, 1208–1229. <https://doi.org/10.1111/j.1365-2486.2006.01150.x>.
- Kang, H.-S., Xue, Y., & Collatz, G.J. (2007). Impact Assessment of Satellite-Derived Leaf Area Index Datasets Using a General Circulation Model. *Journal of Climate*, 20(6), 993–1015. <https://doi.org/10.1175/jcli4054.1>.
- Kalnay, E., Kanamitsu, M. and Baker, W.E. (1990) Global numerical weather prediction at the National Meteorological Center. *Bulletin of the American Meteorological Society*, 71, 1410–1428. [https://doi.org/10.1175/1520-0477\(1990\)071<1410:GNWPAT>2.0.CO;2](https://doi.org/10.1175/1520-0477(1990)071<1410:GNWPAT>2.0.CO;2).
- Kanamitsu, M., Alpert, J.C., Campana, K.A., Caplan, P.M., Deaven, D.G., Iredell, M., Katz, B., Pan, H.L., Sela, J. and White, G.H. (1991) Recent changes implemented into the global forecast system at NMC. *Weather and Forecasting*, 6, 425–435. [https://doi.org/10.1175/1520-0434\(1991\)006<0425:rciitg>2.0.co;2](https://doi.org/10.1175/1520-0434(1991)006<0425:rciitg>2.0.co;2).
- Klein, C., Bliefernicht, J., Heinzeller, D., Gessner, U., Klein, I. and Kunstmann, H. (2017) Feedback of observed interannual vegetation change: a regional climate model analysis for the west African monsoon. *Climate Dynamics*, 48, 2837–2858. <https://doi.org/10.1007/s00382-016-3237-x>.
- Lauwaet, D., Lipzig, N.P.M. and Ridder, K. (2009) The effect of vegetation changes on precipitation and Mesoscale convective Systems in the Sahel. *Climate Dynamics*, 33, 521–534. <https://doi.org/10.1007/s00382-009-0539-2>.
- Lawrence, D.M., Hurtt, G.C., Arneth, A., Brovkin, V., Calvin, K.V., Jones, A.D., Jones, C.D., Lawrence, P.J., de Noblet-Ducoudré, N., Pongratz, J., Seneviratne, S.I. and Shevliakova, E. (2016) The land use model Intercomparison project (LUMIP) contribution to CMIP6: rationale and experimental design. *Geoscientific Model Development*, 9, 2973–2998. <https://doi.org/10.5194/gmd-9-2973-2016>.
- Lawrence, P.J. and Chase, T.N. (2010) Investigating the climate impacts of global land cover change in the community climate system model. *International Journal of Climatology*, 30, 2066–2087. <https://doi.org/10.1002/joc.2061>.
- Lawrence, P.J., Lawrence, D.M. and Hurtt, G.C. (2018) Attributing the carbon cycle impacts of CMIP5 historical and future land use and land cover change in the community earth system model (CESM1). *Journal of Geophysical Research Biogeosciences*, 123, 1732–1755. <https://doi.org/10.1029/2017JG004348>.
- Lee, J., Xue, Y., De Sales, F., Diallo, I., Marx, L., Ek, M., Sperber, K. R., and Gleckler, P.J. (2018) Evaluation of multi-decadal UCLA-CFSv2 simulation and impact of interactive atmospheric-ocean feedback on global and regional variability. *Climate Dynamics*, 52, 3683–3707. <https://doi.org/10.1007/s00382-018-4351-8>.
- Marsh, G.P. (1864) *Man and Nature: Or, Physical Geography as Modified by Human Action*, 1st edition. New York, NY: C. Scribner & Company.
- Meng, X.H., Evans, J.P. and McCabe, M.F. (2014) The impact of observed vegetation changes on land-atmosphere feedbacks during drought. *Journal of Hydrometeorology*, 15, 759–776. <https://doi.org/10.1175/JHM-D-13-0130.1>.
- Moorthi, S. and Suarez, M.J. (1992) Relaxed Arakawa-Schubert: a parameterization of moist convection for general circulation models. *Monthly Weather Review*, 120, 978–1002. [https://doi.org/10.1175/1520-0493\(1992\)120<0978:RASAP0>2.0.CO;2](https://doi.org/10.1175/1520-0493(1992)120<0978:RASAP0>2.0.CO;2).
- Myhre, G., Shindell, D., Bréon, F.-M., Collins, W., Fuglestedt, J., Huang, J., Koch, D., Lamarque, J.-F., Lee, D., Mendoza, B., Nakajima, T., Robock, A., Stephens, G., Takemura, T. and Zhang, H. *Anthropogenic and Natural Radiative Forcing*. In: *Climate Change 2013: The Physical Science Basis*. Contribution of Working Group I to the Fifth Assessment Report of the Intergovernmental Panel on Climate Change [Stocker, T.F., Qin, D., Plattner, G.-K., Tignor, M., Allen, S.K., Boschung, J., Nauels, A., Xia, Y., Bex, V. and Midgley, P.M. (eds.)]. Cambridge: Cambridge University Press.
- Niyogi, D., Subramanian, S., Mohanty, U.C., Kishtawal, C.M., Ghosh, S., Nair, U.S., Ek, M., and Rajeevan, M. (2018) The impact of land cover and land use change on the Indian monsoon region hydroclimate. In: *Land-Atmospheric Research Applications in South and Southeast Asia*. Springer Remote Sensing/Photogrammetry. Cham: Springer.
- Niyogi, D.D.S., Xue, Y. and Raman, S. (2002) Hydrological land surface response in a tropical regime and a midlatitudinal regime. *Journal of Hydrometeorology*, 3, 39–56. [https://doi.org/10.1175/1525-7541\(2002\)003<0039:HLSRIA>2.0.CO;2](https://doi.org/10.1175/1525-7541(2002)003<0039:HLSRIA>2.0.CO;2).
- Paeth, H., Born, K., Girmes, R., Podzun, R. and Jacob, D. (2009) Regional climate change in tropical and northern Africa due to greenhouse forcing and land use changes. *Journal of Climate*, 22, 114–132. <https://doi.org/10.1175/2008JCLI2390.1>.
- Peng, P., Barnston, A.G., and Kumar, A. (2013) A comparison of skill between two versions of the NCEP climate forecast system (CFS) and CPC's operational short-lead seasonal outlooks. *Weather and Forecasting*, 28(2), 445–462. <https://doi.org/10.1175/WAF-D-12-00057.1>.
- Pielke, R.A., Pitman, A., Niyogi, D., et al. (2011) Land use/land cover changes and climate: modeling analysis and observational evidence. *Wiley Interdisciplinary Reviews Climate Change*, 2, 783–934.
- Pillai, P.A., Rao, S.A., George, G., Rao, D.N., Mahapatra, S., Rajeevan, M., Dhakate, A. and Salunke, K. (2017) How distinct are the two flavors of El Niño in retrospective forecasts of climate forecast system version 2 (CFSv2)? *Climate Dynamics*, 48, 3829–3854. <https://doi.org/10.1007/s00382-016-3305-2>.
- Pitman, A.J. (2003) The evolution of, and revolution in, land surface schemes designed for climate models. *International Journal of Climatology*, 23, 479–510. <https://doi.org/10.1002/joc.893>.
- Pitman, A.J., deNoblet-Ducoudré, N., Cruz, F.T., Davin, E.T., Bonan, G.B., Brovkin, V., Claussen, M., Delire, C., Ganzeveld, L., Gayler, V., vanden Hurk, B.J.J.M., Lawrence, P. J., van der Molen, M.K., Müller, C., Reick, C.H., Seneviratne, S. I., Strengers, B.J., and Voldoire, A. (2009) Uncertainties in climate responses to past land cover change: first results from the LUCID intercomparison study. *Geophysical Research Letters*, 36, L14814, 1–6. <https://doi.org/10.1029/2009GL039076>.
- Quesada, B., Devaraju, N., de Noblet-Ducoudré, N. and Arneth, A. (2017) Reduction of monsoon rainfall in response to past and future land use and land cover changes. *Geophysical Research Letters*, 44, 1041–1050. <https://doi.org/10.1002/2016GL070663>.
- Ramu, D.A., Sabeerali, C.T., Chattopadhyay, R., Rao, D.N., George, G., Dhakate, A.R., Salunke, K., Srivastava, A. and

- Rao, S.A. (2016) Indian summer monsoon rainfall simulation and prediction skill in the CFSv2 coupled model: impact of atmospheric horizontal resolution. *Journal of Geophysical Research*, 121, 2205–2221. <https://doi.org/10.1002/2015JD024629>.
- Rodgers, W., Mahmood, R., Leeper, R. and Yan, J. (2018) Land cover change, surface mining, and their impacts on a heavy rain event in the Appalachia. *Annals of the American Association of Geographers*, 108, 1187–1209. <https://doi.org/10.1080/24694452.2018.1460249>.
- Saha, S., Moorthi, S., Wu, X., Wang, J., Nadiga, S., Tripp, P., Behringer, D., Hou, Y.T., Chuang, H.Y., Iredell, M., Ek, M., Meng, J., Yang, R., Mendez, M.P., van den Dool, H., Zhang, Q., Wang, W., Chen, M. and Becker, E. (2014) The NCEP climate forecast system version 2. *Journal of Climate*, 27, 2185–2208. <https://doi.org/10.1175/JCLI-D-12-00823.1>.
- Schilling, K.E., Jha, M.K., Zhang, Y.K., Gassman, P.W. and Wolter, C.F. (2009) Impact of land use and land cover change on the water balance of a large agricultural watershed: historical effects and future directions. *Water Resources Research*, 44 (7). <https://doi.org/10.1029/2007WR006644>.
- Schneck, R. and Mosbrugger, V. (2011) Simulated climate effects of southeast Asian deforestation: regional processes and teleconnection mechanisms. *Journal of Geophysical Research – Atmospheres*, 116 (D11). <https://doi.org/10.1029/2010JD015450>.
- Shukla, J., Nobre, C. and Sellers, P. (1990) Amazon deforestation and climate change. *Science*, 247, 1322–1325. <https://doi.org/10.1126/science.247.4948.1322>.
- Snyder, P.K. (2010) The influence of tropical deforestation on the northern hemisphere climate by atmospheric teleconnections. *Earth Interactions*, 14, 1–34. <https://doi.org/10.1175/2010EI280.1>.
- Song, G. (2013) *Global and Sahel Regional Biophysical Processes, Vegetation Dynamics, and Climate Interactions*. Los Angeles, CA: University of California Los Angeles.
- Sun, L., Wei, J., Duan, D.H., Guo, Y.M., Yang, D.X., Jia, C. and Mi, X.T. (2016) Impact of land-use and land-cover change on urban air quality in representative cities of China. *Journal of Atmospheric Solar-Terrestrial Physics*, 142, 43–54. <https://doi.org/10.1016/j.jastp.2016.02.022>.
- Sy, S., Noblet-Ducoudré, N.D., Quesada, B., Sy, I., Dieye, A.M., Gaye, A.T. and Sultan, B. (2017) Land-surface characteristics and climate in West Africa: models' biases and impacts of historical anthropogenically-induced deforestation. *Sustainability*, 9. <https://doi.org/10.3390/su9101917>.
- Thomas, W.L. (1956) *Man's Role in Changing the Face of the Earth*. University of Chicago Press, Chicago, <https://doi.org/10.2307/2573335>.
- Vitousek, P.M., Mooney, H.A., Lubchenco, J. and Melillo, J.M. (1997) Human domination of Earth's ecosystems. *Science*, 277, 494–499. <https://doi.org/10.1126/science.277.5325.494>.
- Wackernagel, M., Onisto, L., Bello, P., Callejas Linares, A., Susana López Falfán, I., Méndez García, J., Isabel Suárez Guerrero, A. and Guadalupe Suárez Guerrero, M. (1999) National natural capital accounting with the ecological footprint concept. *Ecological Economics*, 29, 375–390. [https://doi.org/10.1016/S0921-8009\(98\)90063-5](https://doi.org/10.1016/S0921-8009(98)90063-5).
- Winckler, J., Reick, C.H., Luyssaert, S., Cescatti, A., Stoy, P.C., Lejeune, Q., Raddatz, T., Chlond, A., Heidkamp, M. and Pongratz, J. (2019) Different response of surface temperature and air temperature to deforestation in climate models. *Earth System Dynamics*, 10, 473–484. <https://doi.org/10.5194/esd-10-473-2019>.
- Xue, Y. (1996) The impact of desertification in the Mongolian and the inner Mongolian grassland on the regional climate. *Journal of Climate*, 9, 2173–2189. [https://doi.org/10.1175/1520-0442\(1996\)009<2173:TIODIT>2.0.CO;2](https://doi.org/10.1175/1520-0442(1996)009<2173:TIODIT>2.0.CO;2).
- Xue, Y. (1997) Biosphere feedback on regional climate in tropical North Africa. *Quarterly Journal of the Royal Meteorological Society*, 123, 1483–1515. <https://doi.org/10.1256/smsqj.54202>.
- Xue, Y., De Sales, F., Lau, W.M., Boone, A., Feng, J., Dirmeyer, P., Guo, Z., Kim, K.M., Kitoh, A., Kumar, V., Pocard-Leclercq, Mahowald, N., Moufouma-Okia, W., Pegion, P., Rowell, D.P., Schemm, J., Schubert, S.D., Sealy, A., Thiaw, W.M., Vintzileos, A., Williams, S.F. and Wu, M.L.C. (2010a) Intercomparison and analyses of the climatology of the west African monsoon in the west African monsoon modeling and evaluation project (WAMME) first model intercomparison experiment. *Climate Dynamics*, 35, 3–27. <https://doi.org/10.1007/s00382-010-0778-2>.
- Xue, Y., De Sales, F., Lau, W.K.M., et al. (2016) West African monsoon decadal variability and surface-related forcings: second west African monsoon modeling and evaluation project experiment (WAMME II). *Climate Dynamics*, 47, 3517–3545. <https://doi.org/10.1007/s00382-016-3224-2>.
- Xue, Y., De Sales, F., Li, W.P., Mechoso, C.R., Nobre, C.A. and Juang, H.M. (2006) Role of land surface processes in south American monsoon development. *Journal of Climate*, 19, 741–762. <https://doi.org/10.1175/JCLI3667.1>.
- Xue, Y., De Sales, F., Vasic, R., Mechoso, C.R., Arakawa, A., & Prince, S. (2010b) Global and seasonal assessment of interactions between climate and vegetation biophysical processes: a GCM study with different land-vegetation representations. *Journal of Climate*, 23, 1411–1433. <https://doi.org/10.1175/2009JCLI3054.1>.
- Xue, Y., Juang, H.M.H., Li, W.P., Prince, S., DeFries, R., Jiao, Y. and Vasic, R. (2004) Role of land surface processes in monsoon development: East Asia and West Africa. *Journal of Geophysical Research D Atmospheres*, 109(D3). <https://doi.org/10.1029/2003jd003556>.
- Xue, Y., Sellers, P.J., Kinter, J.L. and Shukla, J. (1991) A simplified biosphere model for global climate studies. *Journal of Climate*, 4, 345–364. [https://doi.org/10.1175/1520-0442\(1991\)004<0345:ASBMFG>2.0.CO;2](https://doi.org/10.1175/1520-0442(1991)004<0345:ASBMFG>2.0.CO;2).
- Xue, Y. and Shukla, J. (1996) The influence of land surface properties on Sahel climate. Part II: afforestation. *Journal of Climate*, 9, 3260–3275. [https://doi.org/10.1175/1520-0442\(1996\)009<3260:tiolsp>2.0.co;2](https://doi.org/10.1175/1520-0442(1996)009<3260:tiolsp>2.0.co;2).
- Xue, Y. and Shukla, J. (1993) The influence of land surface properties on Sahel climate. Part I: desertification. *Journal of Climate*, 6(2), 2232–2245.
- Yuan, X., Wood, E.F., Luo, L. and Pan, M. (2011) A first look at climate forecast system version 2 (CFSv2) for hydrological seasonal prediction. *Geophysical Research Letters*, 38. <https://doi.org/10.1029/2011GL047792>.
- Zhan, X., Xue, Y. and Collatz, G.J. (2003) An analytical approach for estimating CO<sub>2</sub> and heat fluxes over the Amazonian region. *Ecological Modelling*, 162, 97–117. [https://doi.org/10.1016/S0304-3800\(02\)00405-2](https://doi.org/10.1016/S0304-3800(02)00405-2).

Zhao, M., Pitman, A.J. and Chase, T. (2001) The impact of land cover change on the atmospheric circulation. *Climate Dynamics*, 17, 467–477. <https://doi.org/10.1007/PL00013740>.

### **SUPPORTING INFORMATION**

Additional supporting information may be found online in the Supporting Information section at the end of this article.

**How to cite this article:** Chilukoti N, Xue Y. An assessment of potential climate impact during 1948–2010 using historical land use land cover change maps. *Int J Climatol*. 2021;41:295–315. <https://doi.org/10.1002/joc.6621>